Investigation of the Possible Relation Between Precipitation and Cosmic Ray Flux Using Wavelet Analysis

A Thesis

Submitted for the Degree of

Master of Science (Engineering)

by

Kopal Arora

Engineering Mechanics Unit
Jawaharlal Nehru Centre for Advanced Scientific Research
(A Deemed University)
Bangalore – 560 064

NOVEMBER 2010

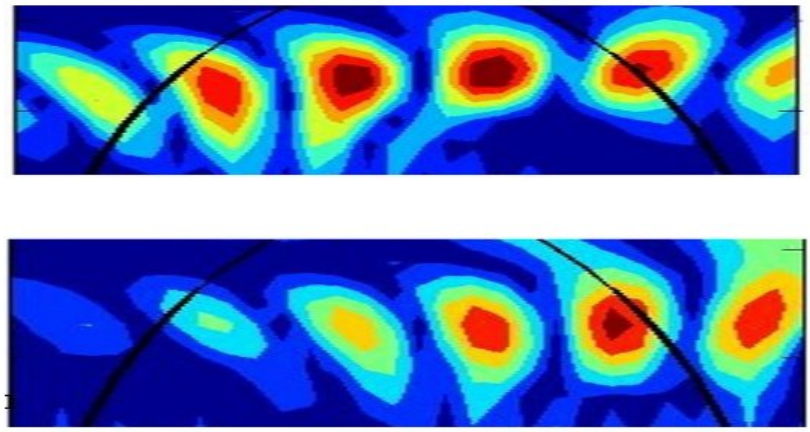

The above illustration presents wavelet maps of the cosmic ray flux (upper panel) and precipitation (lower panel) at the Thule neutron monitor station. The striking similarity in the two maps indicates the strong connections between precipitation and cosmic ray flux at Thule. Note that the use of the wavelet technique enables us to visualize such connections even when the signals are non-stationary and/ or non-linear.

Declaration

I hereby declare that the matter embodied in the thesis entitled, " Investigation of the Possible Relation Between Precipitation and Cosmic Ray Flux Using Wavelet Analysis", is the result of investigations carried out by me at the Engineering Mechanics Unit, Jawaharlal Nehru Centre of Advanced Scientific Research, Bangalore, India, under the supervision of Prof. Roddam Narsimha and Prof.K.R. Sreenivas and that it has not been submitted elsewhere for the award of any degree or diploma.

In keeping the general practice in reporting scientific observations, due acknowledgement has been made whenever the work described is based on the findings of other investigation.

_____

Kopal Arora

Certificate

We hereby certify that the matter embodied in this thesis entitled **"Investigation of the Possible Relation Between Precipitation and Cosmic Ray Flux Using Wavelet Analysis"**, has been carried out by Ms. Kopal Arora at the Engineering Mechanics Unit, Jawaharlal Nehru Centre for Advanced Scientific Research, Bangalore, India under our supervision and that it has not been sumitted elsewhere for the award of any degree or diploma.

Prof. Roddam Narsimha	Prof. KR Sreenivas
(Research Supervisor)	(Research supervisor)

Acknowledgements

It is my pleasure to thank Prof. Roddam Narasimha for his valuable contributions, helpful suggestions and guidance at every stage of this work. And most importantly, his never ending encouragement to do more and his immense patience along with his support through this odyssey. I am fortunate to have him as my advisor.

I wish to acknowledge Prof. KR Srenivas, my other advisor, for posing important questions every now and then which would help me to learn more. And also for important discussions and suggestions regarding academic jobs, which made my stay comfortable in JNC.

I thank prof.Rama govindarajan and Dr. Ganesh Subramanyan who have always been a source of maral support and inspiration. I owe thanks to all the staff and non-staff members for their genuine help and support to the students including me.

My lab mates Ratul, Harish, Anubhab, Priyanka, Ponnu, Srikant, Dinesh, Vivek, Sumesh, Rakshit, Rahul and shivani made my stay homely and delightful. Subarna and Sarita although being senior acted very friendly and gave mental support during the project. I would also like to express thanks to all the students of the department, for lot of fun and keeping lab warm.

I am extremely thankful to Ershaad for being a unconditionally encouraging friend and for being there when I needed the most. And also for helping to work with new softwares which once seemed to be impossible for me to understand. His unwavering support is one I will always appreciate.

Finally, I wish to thank my parents and brothers, the joys of my life, whose support is unconditional.

I personally feel that this work has seen this light of the day by the Grace of God only, to whom I owe everything.

Abstract

The galactic cosmic rays (GCR) are charged particles, primarily protons and helium nuclei. In the present work, by applying data analysis techniques, we have investigated the proposal that GCR can influence precipitation. Wavelet transforms have been applied for the first time to study the problem. This is because the wavelet is the best tool available today to analyse non-stationary and non-linear time series. The method suggests a common 9.8 year cycle in the cosmic ray flux (CRF) and precipitation time series during the considered period [1979-2008] at Thule(76.5 N). Finally, the point process method on wavelet maps has been applied at Thule. The method depicts that CRF leads the precipitation by about 2 and 9 months at Thule.

For the present analysis, six geographically diverse locations across the globe have been selected. The six stations are Thule (76.5 N), Climax (39.4 N), Huancayo (12 S), Namibia (19.12 S), Potchefstroom (26.4 S) and Hermanus (34.25 S); all of them are neutron monitor stations. For the present study, precipitation data have been retrieved from Global Precipitation Climatology Project (GPCP). GPCP blends estimates based on various data sources to produce a global gridded data set, taking advantage of the strengths of each data type. A reliable set of cosmic ray flux data at the six neutron monitor stations mentioned above is available from National Geophysical Data Centre (NGDC). For cloud cover, the data has been extracted from the International Satellite Cloud Climatology Project (ISCCP) archives.

In the present analysis, the correlation between the GCR flux and precipitation has been found to be significantly high at higher latitudes. However, no significant correlation between low cloud cover(LCC) and GCR was detected at any of the six stations. The LCC data was taken from ISCCP. The absence of correlation between the GCR and LCC has been attributed by Svensmark(2003) to calibration problems. Thus, we are not in a position to come to a definite conclusion about the absence or presence of correlation between LCC and GCR.

Using the Fourier power spectrum, a significant 10 year period has been detected in both cosmic ray flux and precipitation at Thule, Potchefstroom and Hermanus. Such a cycle is absent in the precipitation data at Huancayo and Namibia, in the tropics.

One of the ways to explain the physical mechanism underlying a GCR-precipitation

connection can be stated as follows. GCR being charged particles affects the earth's global electrical circuit, and may thus stimulate the formation of charged cloud condensation nuclei (CCN) in the atmosphere. Therefore, higher GCR fluxes would lead to more charged CCN in the atmosphere. It has been noticed[1] that charged CCN are more capable of attracting neutral or oppositely charged ambient particles in the atmosphere. The higher charged-CCN concentrations at times of high GCR fluxes would lead to increased ice nucleation which eventually enhances the precipitation release in cold clouds[2]. This mechanism is expected to be stronger at the higher latitudes due to low geomagnetic cutoff value. Thus, the concentration of GCR is higher at higher latitudes, as in case of Thule, where cold clouds are common and ice nucleation in cold clouds helps in precipitation.

Thus the higher correlation coefficient and the presence of a common 9.8 year cycle in both CRF and precipitation time series at Thule, using power spectrum and wavelet power spectrum method, supports the above mechanism.

Kniveton and Todd in 2001 proposed a relation between the CRF, precipitation and precipitation efficiency. Using data from 1979 to 1999 they found evidence of statistically strong relationships between the three variables over ocean surfaces at mid to high latitudes. Our work confirms their conclusion. In addition, we found non-stationrity and non-linearity in the precipitation time series, and used the wavelet transform in our analysis. Moreover, the 9.8 year cycle in precipitation and CRF time series has been found. Here, we find that CRF leads precipitation by 2 months at Thule.

[1] Yu and Turco 2000

[2] Meteorology today: an introduction to weather, climate, and the environment by C. Donald Ahrens

List of Figures

List of Tables

Contents

CHAPTER 1

INTRODUCTION, MOTIVATION AND LITERATURE REVIEW

Cosmic rays, which are charged particles, are capable of inducing ionization in the atmosphere. This process can explain the formation of condensation nuclei which cluster together into complex ions and aerosols, which is the mechanism of cloud formation on the micro scale. This is despite the minute amount of energy contributed by the cosmic rays to the atmosphere. This may be taken as evidence that cosmic rays amplify the effect of solar energy[1] and provide the missing link in the association between solar activity and climate.

In order to unravel the mystery of the heliosphere's influence on the climate of the earth, it is essential to analyse the variation of climatic variables with that of cosmic proxies for instance, the variation of temperature, precipitation, cloud cover and ENSO with solar activity, cosmic ray flux and so on. The trails of ionization in the atmosphere caused by cosmic rays create condensation nuclei on which cloud droplets can form. This idea has sparked much debate among scientists and attracted much media attention since it was proposed by Svensmark and his colleagues.[2] They showed that, since 1964, galactic cosmic-ray intensity has declined by about 3.7%, and that the trend indicates that the decline could have been going on since the early twentieth century. This, they argue, could account for a significant contribution to the global warming that has occurred over the past 100 years.

The cloud chamber has proved very useful in understanding the cloud condensation mechanism in laboratory experiments. Invented by C.T.R. Wilson at the beginning of the twentieth century, the cloud chamber had initiated a new area of research promising to reveal the mysteries of atmospheric condensation. The

[1]Harrison and Carslaw-2003, Rev.Geophysics, "ion-aerosol-cloud processes in the lower atmosphere", 41, doi:10.1029/2002RG000114

[2]Marsh.N. and Svensmark.H.-2000 Space Science Review,"Low cloud properties influenced by cosmic rays

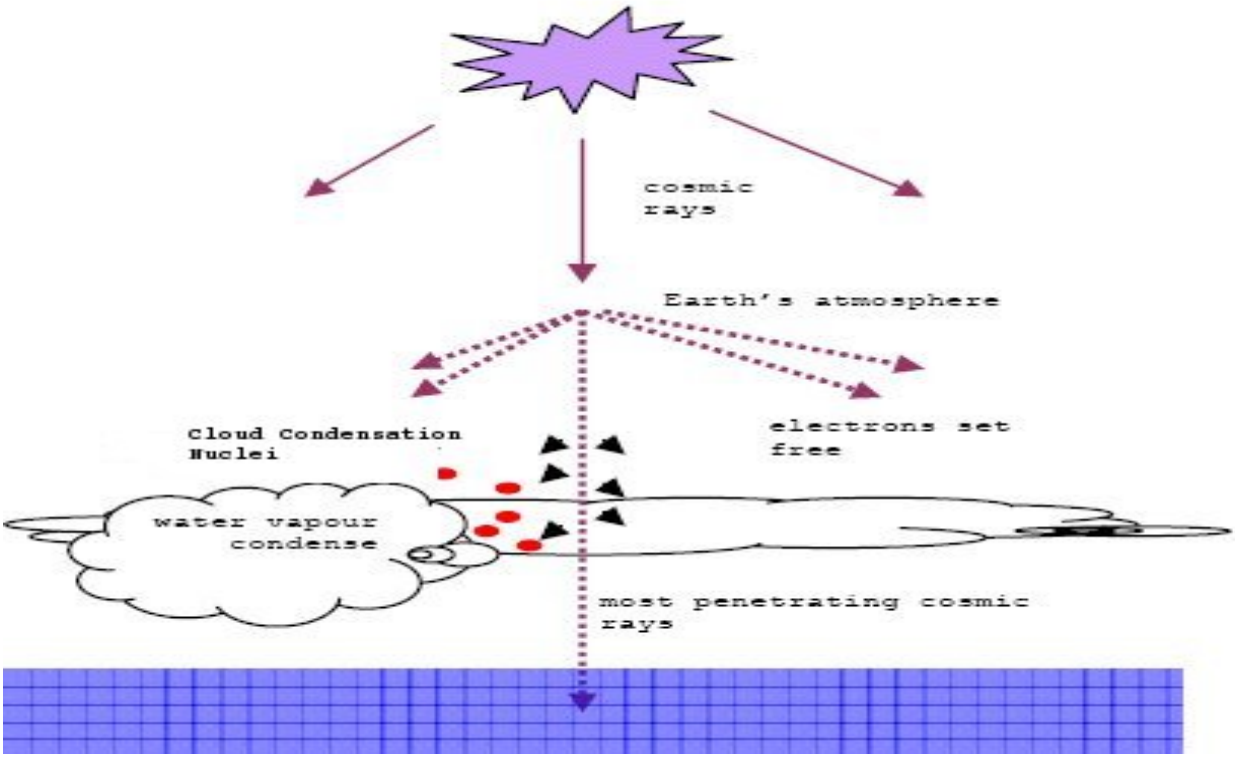

Figure 1.1: Effect of cosmic rays on earth's atmosphere

phenomenon of water droplets coalescing around ions in a chamber saturated with water vapour allowed scientists to visualize the tracks left by the charged particles.

A possible sequence of events connecting cosmic rays to Earth's climate is as follows:

1) A giant star explodes in a supernova and emits cosmic rays,

2) cosmic rays enter the Earth's atmosphere,

3) and release free electrons which act as catalysts for cloud condensation nuclei,

4) on which water vapour condenses into clouds.

The procedure detailed above is illustrated in the figure(1.1)[3]:

Precipitation plays a fundamental role in atmospheric dynamics by influencing atmospheric circulation. It achieves this by spreading energy to the surrounding air in the form of latent heat, released in the condensation process.[4] The objective of this thesis is to investigate the possible connections between precipitation and

[3] *http : //www.junkscience.com/Greenhouse/Cosmic_rays_and_climate.html*

[4] Dominic R. Kniveton and Martin C. Todd, Geophysical Research Letters,2001 "On the relationship of cosmic ray flux and precipitation"

cosmic rays. And also to analyse their correlation with varying latitude.

1.1 Literature Review

The aim of the present work is to detect possible connections between cosmic ray flux, originating from extragalactic sources, and two atmospheric parameters, namely precipitation and cloud cover. The hypothesis that cosmic rays can influence cloud cover has sparked much debate in the last 15 years. The primary idea behind the hypothesis is that galactic cosmic ray flux incident on the earth may affect cloud cover by influencing ionization and hence causing microphysical changes in the atmosphere. In particular, nucleation and growth of ice particles may change too. In 1995, Pudovkin[5] found that a short term decrease in galactic cosmic ray flux due to increased solar activity, known as forbush decrease, can cause local reduction in the amount of cloud cover. However, he found that the effect disappears at latitudes lower than $55\,^{\circ}$.

The cloud-cosmic theory proposed by Friis-Christensen and Svensmark in 1997[6] claimed to observe a strong correlation between the variation in global cloud cover and the cosmic ray flux. They found that from 1987 to 1990, global cloudiness dipped by approximately 3% when the number of cosmic ray particles reaching the earth fell by 3.5%., a fluctuation that matched with a peak in sunspot numbers to 4%, during higher solar activity.

Later in 1998, H. Svensmark reported in Physical Review Letters[7] that earth's mean temperature follows the decadal variations in galactic cosmic ray flux and solar activity more closely than other solar activity parameters, and concluded that the heliosphere affects earth's climate.

A study in 2000 by ND Marsh and H. Svensmark in Physical Review Letters, 2000 APS, reported that their observations indicated a possible mechanism for the influence of solar modulated cosmic ray flux on global cloud cover. Moreover, they found that the influence of solar variability was strongest on low clouds (altitude $\leqslant 3$ km); this points to the enhancement of the microphysical mechanism leading

[5]MI Pudovkin, SV Veretenenko - Journal of Atmospheric and Terrestrial,1995 " Cloudiness decreases associated with Forbush decreases in galactic cosmic rays, 57(11),13491355"

[6]H Svensmark, E. Friis-Christensen, Journal of Atmospheric and Solar, 1997,"Variation of cosmic ray flux and global cloud coveragea missing link insolar climate relationships

[7]H. Svensmark 1998 APS Phys. Rev. Lett.,Influence of cosmic rays on earths climate $81, 50275030$

to aerosol formation as a result of the ionization due to cosmic rays. Cosmic ray flux seems to provide the missing link between solar activity and cloud cover. They asserted that the average state of the heliosphere is important for climate on Earth[8].

Interestingly in 2002 another side of cosmoclimatology[9] came into the picture. Nir Shaviv of the Canadian Institute for Theoretical Astrophysics, University of Toronto[10] found that the occurrence of ice-age epochs appears to have non trivial correlation with the spiral arm crossing and hense the cosmic ray flux variability. The galaxy's spiral arm consist of dense massive stars, which explode over tens of millions of years as supernovae. Since supernovae are thought to be the source of cosmic rays, the Sun's passage through a spiral arm would mean greater cosmic-ray exposure, more clouds, and consequently, lower temperatures for Earth. Shaviv thus argued that these periodic crossings and the high cosmic-ray flux they bring with them, correspond to four major ice-age epochs on the earth. The coincidence of the cosmic rays with the ice-age epochs would mean that the climate on earth depends on the solar neighbourhood. Actually, this idea was proposed in 1921 by the American astronomer Harlow Shapley, who suggested that 80% of the variation in the sun's activity is due to the interstellar clouds, which would influence the earth.

A similar idea was proposed by McCrea1, Shapley and Hoyle and Lyttleton[11] suggesting that passages of the solar system through interstellar clouds have appreciable effects on the earth.

However, the treatment of data in the manner H. Svensmark did has been questioned. An article published in 2004 in *Eos* by Paul Damon of the University of Arizona in Tucson and Peter Laut of the Technical University of Denmark discussed several examples of apparently unacceptable handling of observational data which exaggerated the correlation. They also pointed arithmetical errors and noted that the cloud data that had been used originally did not represent total global cloud cover. With corrected data, the correlation broke down. Thus, it was apparent that Svensmark was using a different measure of cloudiness, and argued that the

[8]ND Marsh, H Svensmark - Physical Review Letters, 2000-APS "Low cloud properties influenced by cosmic rays"

[9]The name proposed by H. Svensmark

[10]Shaviv, N. J. Phys. Rev. Lett. 89, 051102 (2002), "Cosmic ray diffusion from the galactic spiral arms, iron meteorites, and a possible climatic connection".

[11]Galactic dust lanes and lunar soil, Nature 257, 776 - 778 (30 October 1975); doi:10.1038/257776a0

new measure made more sense than the original one, as the revised data seemed to be influenced by the cosmic rays.

I.G. Usoskin, N.Marsh, G.A. Kovaltsov, K.Mursula, O.G. Gladysheva in 2004, studied the connection of the global distribution of the observed low cloud amount and the *calculated* tropospheric ionization induced by cosmic rays. They noticed a significant correlation between the annual cosmic ray flux and the amount of low clouds for a period of 20 years. After using de-trended data, the correlation appeared to be $0.90(> 99\%)$ in mid latitudes$(60\,^{\circ}Sto25\,^{\circ}S$ and $25\,^{\circ}Nto70\,^{\circ}N)$, $0.84(> 99\%)globally(60\,^{\circ}Sto70\,^{\circ}N)$ and in tropics, $0.61(94\%)$.

In 2006, he experimentally demonstrated the formation of small aerosol particles by the incident ionizing particles, considered as proxies to cosmic rays. In 2007, H Svensmark, named the cosmic - cloud phenomenon as cosmoclimatology in a paper published in Astronomy and Geophysics. His theory examines the effect of cosmic rays on three different types of clouds, viz- low , High and middle. Svensmark with his colleagues experimentally found that cosmic rays being highly ionizing radiation can create ultra-small aerosol particles which in turn can act as condensation nuclei for cloud formation.

In 2008, T. Sloan and A.W.Wolfendale disagreed with the cosmic−cloud hypothesis,showing that in some places, the cloud cover is anti−correlated with the cosmic ray flux, which is contrary to what is expected. At the 95% confidence level, they claim that less than 23% of the changes of the cloudiness during the 11-year cycles is caused by cosmic rays. Interestingly, in 2001, Knivetion and Todd proposed a link between the cosmic ray flux, precipitation and precipitation efficiency. Using global data from 1979 to 1999, they found evidence of a statistically strong relationship between cosmic ray flux, precipitation and precipitation efficiency over ocean surfaces at mid to high latitudes. Both precipitation and precipitation efficiency, the efficiency with which atmospheric moisture is converted to precipitation, are shown to vary by 79 percent during the solar cycle of the 1980s over the latitude band 45 90°S. In contrast, alternative explanations of the variation in these atmospheric parameters involving changes in tropospheric aerosol content and El Nino Southern Oscillations show poorer statistical relationships with precipitation and precipitation efficiency. Variations in precipitation and precipitation efficiency, potentially caused by changes in cosmic ray flux have implications for the under-

standing of cloud and water vapour feedback. [12]

1.2 Present work

To check the cosmioclimatology theory proposed by Svensmark, we applied the method of correlation coefficient to find the strength of the influence of cosmic rays on aerosols. As a reliable set of aerosol data was available for only a short duration, from march 2000 to December 2008, we can not confirm the correlation significantly. However, we could not find any significant correlation at any of the six stations situated at different latitudes and longitudes. Further, we employed the method of correlation coefficient to detect any relation between the ionizing cosmic rays and cloud cover. But, no significant relation was found by Sloan, who considered cosmic ray intensity in the period from 1985 to 2005. Harrison of Reading University, who studied the effect of cosmic rays in the UK, emphasized that their work provides an upper limit on the cosmic ray-cloud effect in global satellite cloud data.[13]. However, no satisfactory conclusion could be made regarding the cloud cosmic connections.

In order to identify the influence of cosmic rays on low cloud cover, we have selected six locations at varying latitude and longitude. At none of the six locations, Thule(in Northern hemispher), Climax, Potchefstroom and hermanus(mid latitude), Huancayo and Namibia(tropics), was a significant correlation between the cosmic rays and low cloud cover detected in a 13 to 14 year period, for data sets ranging from either 1994 to 2006 (for Huancayo and Climax)or between 1994 to 2007(Climax, Potchefstroom, Thule and Hermanus).

With the advent of advanced mathematical techniques, it is possible to detect the periodicities in non-stationary signals as well. In the present work, we exploit a potent mathematical tool, Wavelet analysis, to detect important periodicities hidden in the signal. Here, we have found the non-stationary nature of the cosmic and climatic signals, using wavelets, along with the periodicities in the time series mentioned before. Moreover, significantly higher correlation between the cosmic ray flux and precipitation is observed at higher latitudes and the poles.

[12]Dominic R. Kniveton and Martin C. Todd, Geophysical Research Letters,2001,"On the relationship of cosmic ray flux and precipitation" VOL. 28 NO. 8,PP. 1527-1530

[13]Harrison Giles; Stephenson David,Proceedings of the Royal Society A: Mathematical, Physical and Engineering Sciences(2008) "Empirical evidence for a non-linear effect of galactic cosmic rays on clouds".

In order to study the relation between cosmic ray flux and precipitation, we have considered six locations across the globe, varying in latitude and longitude. Various mathematical techniques, beginning from correlation coefficient at a suitable significance level, followed by weltch power spectrum and finally wavelet analysis, show a significant relation between the cosmic ray flux and precipitation in the *N. hemisphere*. However, anti-correlation was found at the tropics, *Huancayo* neutron monitor station, in accordance to the roughly positive relation of the precipitation with the sunspots which is in turn negatively related to the cosmic rays.

1.3 References

- Damon, P. E. and Laut, P. Eos , "Pattern of strange errors plagues solar activity and terrestrial climate data."85, 370374 (2004)

- NATURE—Vol 443—14 September 2006- NEWS FEATURE

- Nir J. Shaviv : Phys. Rev. Lett.-2002 , "Cosmic Ray Diffusion from the Galactic Spiral Arms, Iron Meteorites, and a Possible Climatic Connection" 89, 051102 (2002) [4 pages]

- D. R. Gies and J. W. Helsel; "Ice Age Epochs and the Sun's Path through the Galaxy"; The Astrophysical Journal ;Issue:Volume 626, Number 2,2005$March$14

- MI Pudovkin, SV Veretenenko 1995,Journal of Atmospheric and Terrestrial,1995 " Cloudiness decreases associated with Forbush decreases in galactic cosmic rays", 57(11),13491355

- H Svensmark, E. Friis-Christensen, Journal of Atmospheric and Solar, 1997, "Variation of cosmic ray flux and global cloud coverage– a missing link in solar climate relationships"

- H. Svensmark 1998 APS Phys. Rev. Lett.,"Influence of cosmic rays on earth's climate" 81, 50275030

- ND Marsh, H Svensmark - Physical Review Letters, 2000 "Cosmic rays, clouds, and climate " - APS

- McCrea1, Shapley and Hoyle and Lyttleton- 1975, Nature, “Galactic dust lanes and lunar soil”, 257, 776 - 778 (30 October 1975); doi:10.1038/257776a0

- Harrison Giles; Stephenson David, Proceedings of the Royal Society A: Mathematical, Physical and Engineering Sciences(2008), ”Empirical evidence for a non-linear effect of galactic cosmic rays on clouds”.

- Dominic R. Kniveton and Martin C. Todd, Geophysical Research Letters,2001 ”On the relationship of cosmic ray flux and precipitation”

CHAPTER 2

THE DATA ANALYSED

2.1 Cloud Cover

Cloud cover (also called cloud fraction) describes the fraction of the sky covered by clouds. It is measured either as a percentage, or as a fraction ranging from 0 to 1.0. For our analysis, we have considered only low clouds, as a significant correlation between low clouds and cosmic ray flux has been found by Marsh and Svensmark.

2.1.1 Low Cloud Cover

A basis of classification of clouds is by three broad altitude ranges, where different cloud types are associated with each range. The measure of the cloud's altitude which is often called cloud top or effective cloud height, is sensed and used in satellite observations as well. However, a satellite can not directly identify a cloud type due to the absence of qualitative information about cloud structure. However, information about cloud type can be obtained by analysing radiance measurements obtained from the satellites. [1] The low cloud data, used in our analysis, has been taken from the MY NASA DATA Live Access Server (LAS), which in turn is derived from ISCCP, International Satellite Cloud Climatology Project, which was established in 1982 as part of the World Climate Research Program (WCRP) [2]

Further, we consider six geographically diverse locations across the globe. The raw low cloud cover data has been illustrated in figure (2.1), which spans varying meteorological subdivisions. The selection of stations is based upon the availability of reliable cosmic ray flux data.

[1] Ref: NASA Atmospheric Sciences Data Center $http://eosweb.larc.nasa.gov/$ and $http://mynasadata.larc.nasa.gov/glossary_LAS.php?lascategory = Cloud\%20Coverage$

[2] Data source:
$http://isccp.giss.nasa.gov/products/isccpDsets.html$

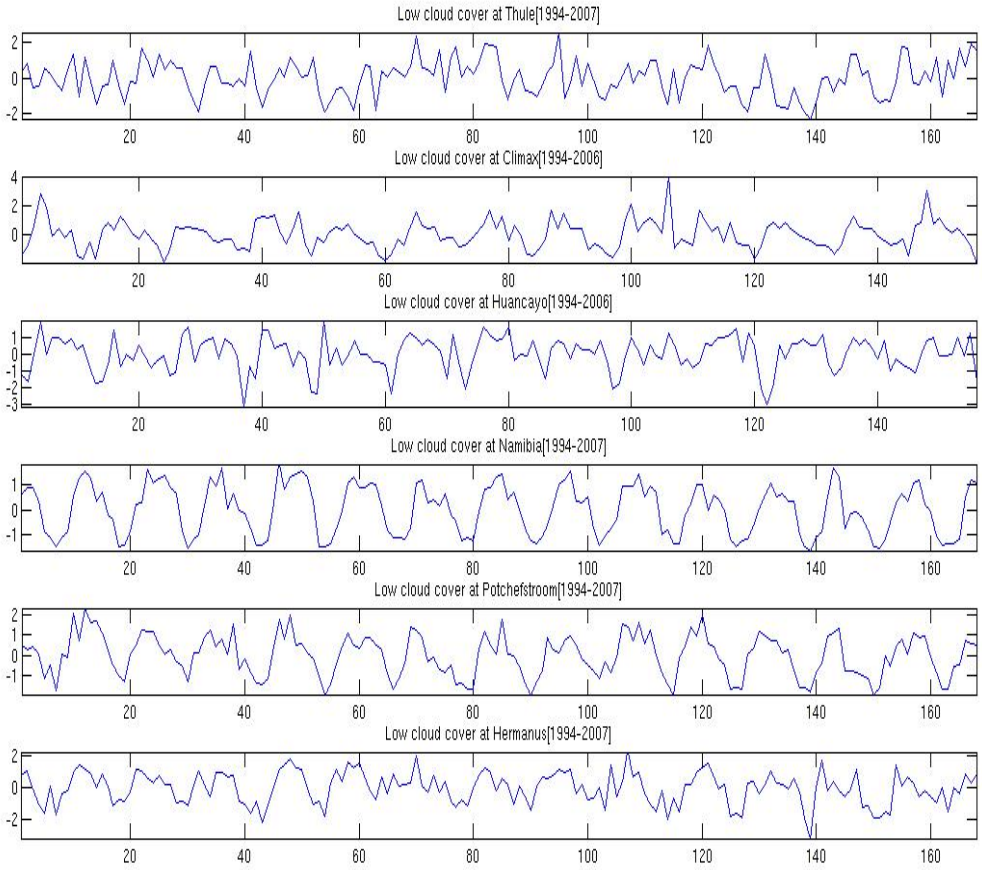

Figure 2.1: Normalized monthly Low cloud cover time series at six different locations across the globe. X-axis represents the time in months since January 1994 to December 2007. And Y-axis refers to the normalized low cloud amount

2.2 Precipitation

Precipitation is liquid or frozen water (rain or snow) produced by weather systems. Precipitation is expressed in units of depth, or height of accumulation (mm, inches) falling on the surface of the earth, e.g. water that falls on an area or a collector (rain gauge) to a measured depth. Precipitation data used here is expressed as the amount of water that falls in a given time period, e.g. mm/day.

The dataset is a combined observation dataset, that is, a gridded analysis based on gauge measurements and satellite estimates of rainfall. The Global Precipitation

Climatology Project (GPCP) combines the various estimates together to produce the necessary global gridded data, taking advantage of the strengths of each data type. The microwave estimates are based on Special Sensor Microwave/Imager (SSM/I) data from the Defense Meteorological Satellite Program (DMSP, United States) whose satellites that fly in sun-synchronous low-earth orbits. The infrared (IR) precipitation estimates are computed primarily from geostationary satellites (United States, Europe, Japan), and secondarily from polar-orbiting satellites (United States). Additional low-Earth orbit estimates include the Atmospheric Infrared Sounder (AIRS) data from the NASA Aqua, and Television Infra-red Observation Satellite Program (TIROS) Operational Vertical Sounder (TOVS) and Outgoing Long wave Radiation Precipitation Index (OPI) data from the NOAA series satellites. The gauge data are assembled and analysed by the Global Precipitation Climatology Centre (GPCC) of the Deutscher Wetterdienst and by the Climate Prediction Center of NOAA.[3]

The currently operational procedure to produce the GPCP precipitation data, which is a Combined Precipitation Data Set, is described in Adler et al (2003), covering the period from January 1979 through to the present. The data can be found at the Global Precipitation Climatology Project (GPCP) web page.[4] [5]

In this thesis, annual precipitation time series at a set of six selected meteorological stations, is used for analysis. The selection is based on the availability of a reliable data set, coverage of different latitudes and longitudes. The data are displayed in figure (2.2). It may be noted that, before analysis the time series have been standardized, by subtracting the mean and dividing by the standard deviation of the data set. The data are presented in that form. Further, monthly time series are presented in the Figure (2.3).

[3] $http://precip.gsfc.nasa.gov/gpcpv2.1data.html$

[4] $http://precip.gsfc.nasa.gov/gpcpv2.1data.html$

[5] NOTE: Duration of the Precipitation or the cloud cover data has been chosen according to the availability of the cosmic rays data set

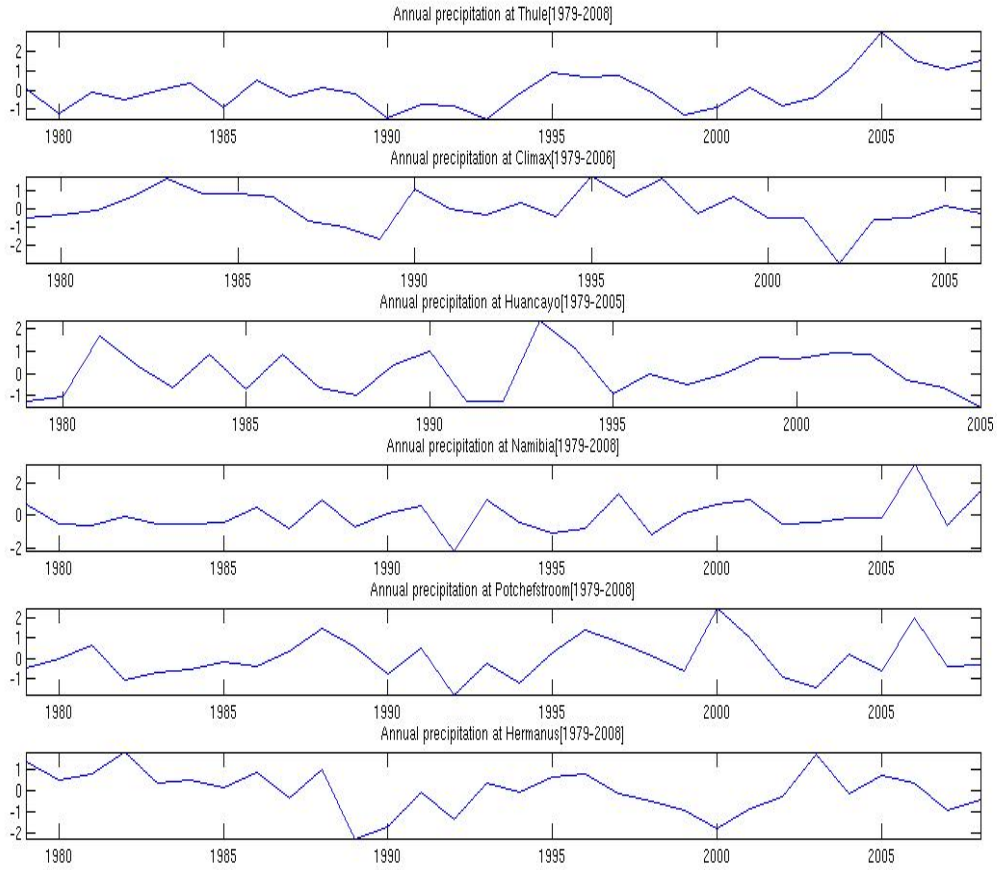

Figure 2.2: Normalized annual precipitation time series at six different locations on the globe. X-axis represents the duration of data from 1979 to 2008 and Y-axis shows the normalized precipitation amount

2.3 Cosmic Rays

Neutron count has been used as a measure for the cosmic ray flux in the present analysis. The cosmic rays, being charged particles interact with the earth's atmosphere and ionize the air into several nuclear particles. The phenomenon of the cascading production of secondary particles by the primary cosmic rays, originating from outer space, is called a *shower*, see figure (2.4)[6]. The collision of the cosmic

[6]The figure has been taken from
$http://www.ngdc.noaa.gov/stp/SOLAR/COSMICRAYS/image/shower.gif$

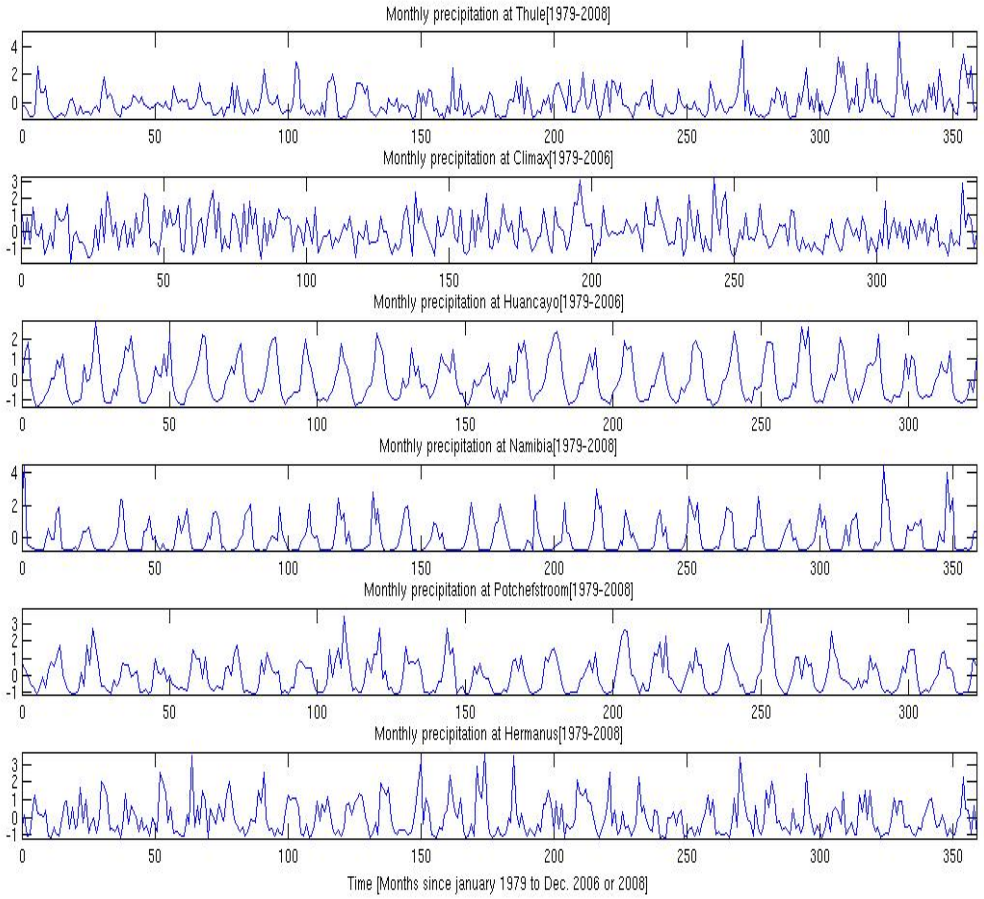

Figure 2.3: Normalized monthly precipitation time series at six different locations at the globe

rays with atmospheric nuclei produces pions, kaons, and unstable mesons that decay to muons. A few of these muons do not interact with atmospheric particles, and because of the relativistic effect of time dilation are able to reach the earth's surface. As muons are charged particles, they can be detected by particle detectors, such as for instance muon detectors, scintillation counters, bubble chambers and so on. However, the neutrons produced in secondary ionization are detected far more efficiently by neutron monitors, which detect particles in the energy range of 500MeV to 20GeV, and are capable of measuring the flux of particles varying between 500 to $4GeV$ energy. The neutron monitors have polyethylene slabs and

lead casing, which are hit by the neutrons produced in the atmosphere.

$$O + p \rightarrow n + \pi \tag{2.1}$$

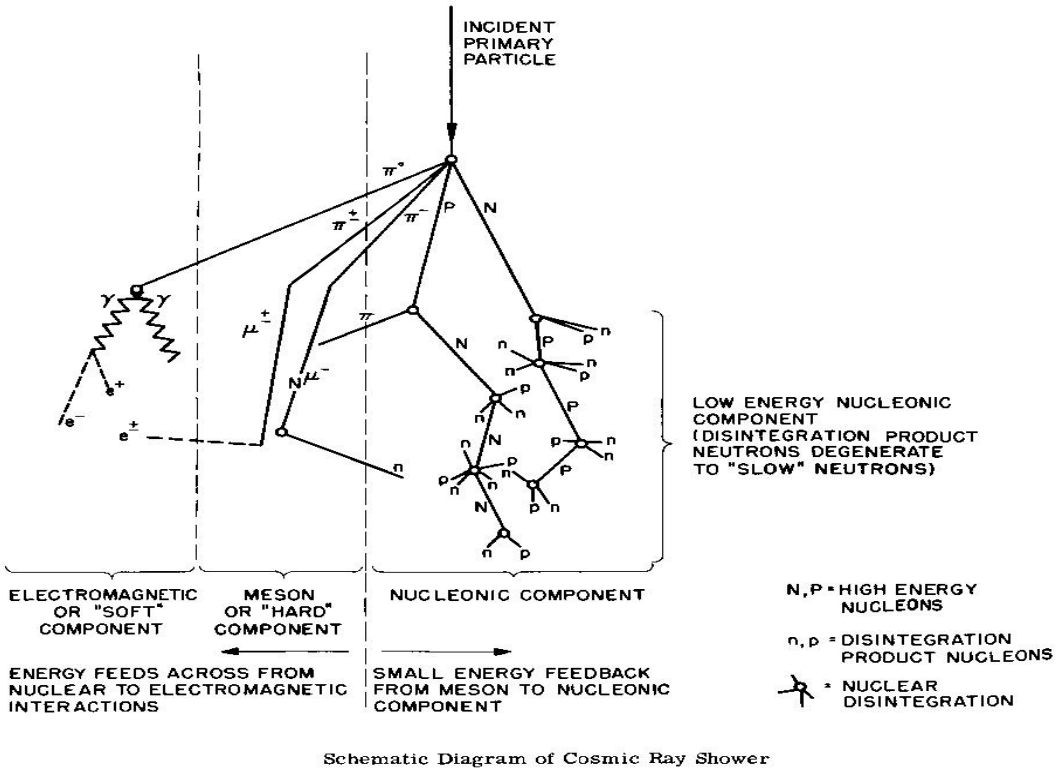

Figure 2.4: A schematic diagram illustrating Air Shower

2.3.1 Variations of Cosmic Rays with Latitude

As explained at the NGDC's cosmic rays link[7], the geomagnetic cut-off is low at higher latitudes and high at lower latitudes. The lower threshold response of the neutron monitor is controlled by the atmospheric mass which limits the response threshold of the neutron monitor to primary radiation of about 430 Mega electron Volts (MeV). For instance, at the south pole, where the surface is about 2820 m above sea level, the reduced atmospheric mass lowers the primary radiation detection threshold to about 300(MeV)). At equatorial latitudes, the detection

[7] $http://www.ngdc.noaa.gov/stp/SOLAR/COSMIC_RAYS/cosmic.html$

threshold is controlled by the geomagnetic cut-off. Thus, it is well understood that the count rate at the poles will be much higher than that in the tropics, owing to high cut-off rigidity. Apart from the latitude, the altitude of the station also influences the neutron monitor count; high altitudes show higher counting rates than lower altitudes because of the atmospheric absorption of the cosmic ray secondaries generated near the top of the atmosphere. The normalized value of the cosmic ray flux variable is similar but not exactly the same. Thus, to avoid any error which might occur due to small variations in the neutron count, the data at six neutron monitor stations have been analysed. But as the normalized values of the cosmic rays flux variation in time at different latitudes are similar, and to compensate the scarcity of the cosmic ray data at isolated places and over oceans, a well organised and continuous data set at a station has been considered as the proxy for the cosmic ray flux at all other locations by quite a few scientists[8].

2.3.2 Neutron Monitor Stations:

List of neutron monitor stations world wide is shown in Table (2.1), and the stations are marked on a map in figure (2.6)[9]. The stations considered for analysis are also indicated in figure (2.6). The choice of the stations is governed by the latitude coverage and the availability of data. Since, there are not many stations across the globe and a few have continuous and reliable data set we do not have much choice to select the stations. There is no station between Huancayo and Climax with continuous and reliable data set. Thus, there is a large gap in latitude between Huancayo and Thule.

2.3.3 Pressure Correction

The counting rates are corrected for atmospheric pressure effects. The cosmic ray data are pressure corrected by multiplying a standard coefficient of 0.95 per mm-Hg, computed taking into account the correlation between the time changes of the barometric coefficient and the modulation of the nucleonic intensity. The secondary

[8]H Svensmark, E. Friis-Christensen: Journal of Atmospheric and Solar-Terrestrial Physics, 1997; Dominic R. Kniveton and Martin C. Todd, Geophysical Research Letters,2001,"On the relationship of cosmic ray flux and precipitation" VOL. 28 NO. 8,PP. 1527-1530

[9]$Source : http://ulysses.sr.unh.edu/NeutronMonitorimages/0_WorldNeutronMonitors.gif$

particles, owing to absorption by a thick and dense atmosphere, are very sensitive to the atmosphere above the neutron monitor. Dense atmosphere corresponds to more absorption of the secondaries and vice-versa. As a result, a lower counting rate is observed at the places with higher pressure or denser atmosphere above them. Pressure correction at every location depends on the pressure above the monitor. The pressure dependence of the particle is expressed as[10]
$N = N_0 \ \exp[-b(P - P_0)]$
where P is pressure and P_0 is a reference pressure (both in mm Hg), usually the average station pressure. N and N_0 are the counting rates at P and P_0 respectively. The quantity b, called the barometric coefficient, has a value of about 0.1% percent per mm Hg *i.e.* a pressure increase (decrease) of 1 mm Hg leads to a decrease (increase) of 0.1 in the neutron monitor counting rate. Neutron monitors with typical counting rates of the order of 106 counts per hour have statistical uncertainties of 0.3 to 0.1 percent. This implies that one must attempt to correct for pressure induced variations in counting rates to at least this level of accuracy. With $b = 1$ percent per mm Hg, it follows that atmospheric pressure must be known accurately to about 0.1 to 0.3 mm Hg.

2.4 Solar Activity

2.4.1 Computing Sunspot Number Data

In order to compute the sunspot number, firstly, the sunspot groups are multiplied by 10 and then added to the individual number of spots counted. This technique of computing the sunspot number is a traditional one, as used by Rudolf Wolf during the 1840's (and hence known by his name). It is worth mentioning that he successfully computed the solar activity cycle to be 11.1 years by using historical records. Moreover, Wolf independently found that the geomagnetic field has a connection with the solar activity. The sunspots evolve unevenly across the solar longitudes, and as the sun rotates the number of sunspots counted varies with the location of observation on the earth. In order to compensate for these limitations,

[10]Chilingarian A., and Karapetyan T.,Calculation of the barometric coefficients for the particle detectors belonging to the world-wide networks at the start of the 24-th Solar Activity cycle,Proceedings of $FORGES-2008$ conference, in press.

a weighted average of measurements is taken from a network of cooperating observatories and it is this weighted average which is considered as an internationally accepted number.

An 11.1 year cycle is a well known cycle during which the sunspot numbers rise and fall. Interestingly, the sunspot cycle is asymmetric, as it takes about 4.8 years to rise from minimum to a maximum value and then 6.2 years to fall back to a minimum value[11].

The data considered here ranges from January 1979 to December 2008. This cover two full cycles (21 st and 22nd solar cycles) and partially covers 20 th and 23 rd solar cycles. Complete 21st and 22nd solar cycles are short duration cycles of an average of 10 years on an average [12]. Thus, the period of 10 years found in the CRF time series can be accounted by the solar cycle during the period.

The sunspot data has also been standardized before being analysed. The figure (2.8) shows the variation of the sunspot number during the period from January 1979 to December 2008. The period is the same as that considered for cosmic ray flux and precipitation data.

2.5 Discussion

The precipitation data has been taken from the Global Precipitation Climatology Project (GPCP) data set. The data considered is the most reliable available to date in contrast to the data used in a very well known paper by Kniveton and Todd, who used climate prediction center merged analysis of precipitation (CMAP) data whose reliability is disputed[13].

[11]National Geophysical Data Center, NGDC

[12]S.K. Pandey, Rahul srivastave, LK borkar, AK tripathi, Aka tripathi and SC dubey, Research Communications, Current Science 10June 2010, "Study of sunspots and sunspot cysles 1-24", Vol.98, No.11

[13]Comparison of Globally Complete Versions of GPCP and CMAP Monthly Precipitation Analyses",Curtis, Scott Adler, Robert Huffman, George

Churchill.NM
Climax.NM
DeepRiver.NM
Ellsworth.NM
Fairbanks.NM
Freiburg.NM.
Goettingen.NM.
HeissIsland.NM
Hermanus.NM
Herstmonceux.NM.
Huancayo.NM
Irkutsk.NM
Irkutsk.NMK.
Jungfraujoch.NM.
Kiel.NM.
Kodaikanal.NM.
Lae.NM
Leeds.NM
Lincoln.NM
Lindau.NM.
Lomnicky.NM.
London.NM.
MakapuuPoint.NM.
Makerere.NM.
Mawson.NM.
MinaAguilar.NM
Mirny.NM
Moscow.NM.
MtNorikura.NM.
MtWashington.NM.
MtWellington.NM.
Munich.NM.
MurchisonBay.NM.
Murmansk.NM.
Namibia.NM
Nederhorst.NM.
Northfield.NM.
Ottawa.NM.
PicDuMidi.NM
Potchefstroom.NM
Prague.NM.
ResoluteBay.NM
RioDeJaneiro.NM.
Rome.NM.
SulphurMt.NM
Thule
Uppsala.NM
Ushuaia.NM
Weisenau.NM.

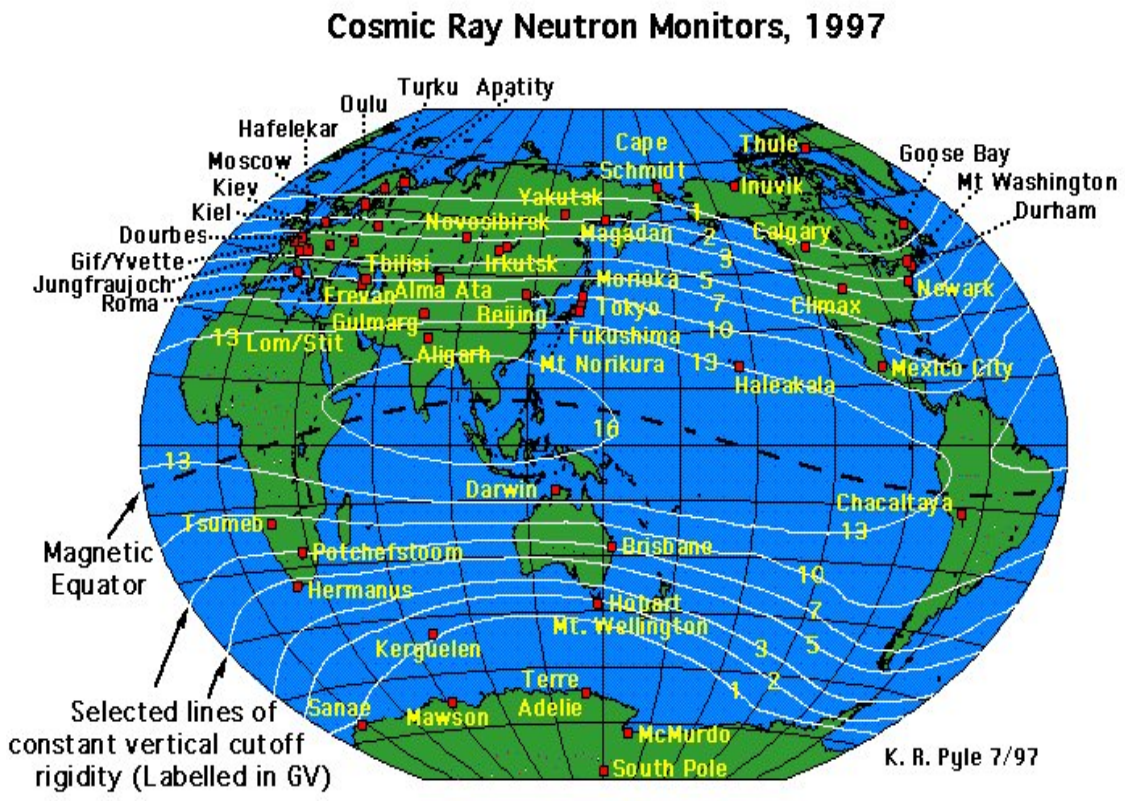

Figure 2.5: Neutron Monitor Stations across the globe

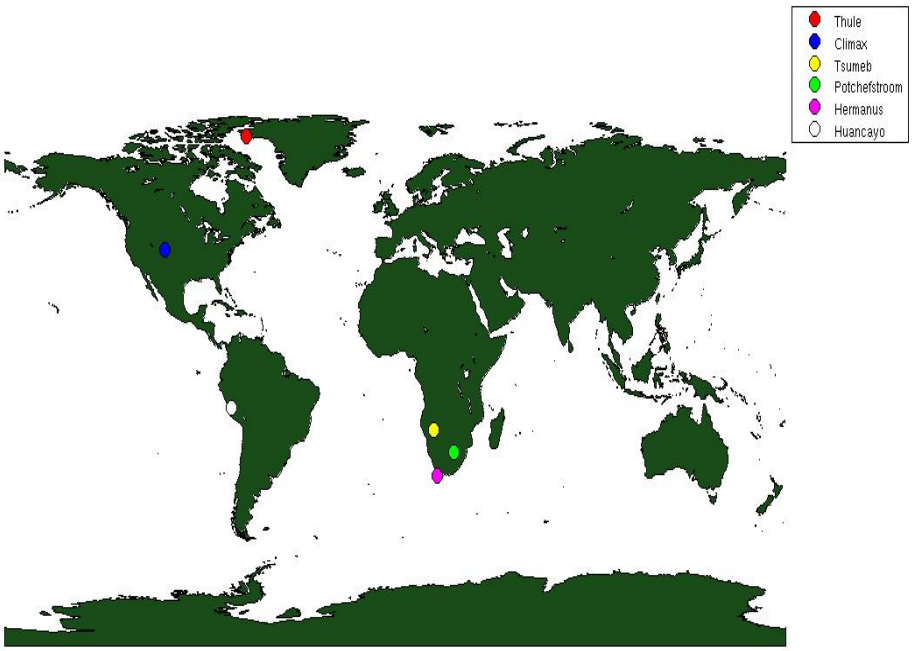

Figure 2.6: Location of the six Neutron Monitor Stations considered for the Analysis

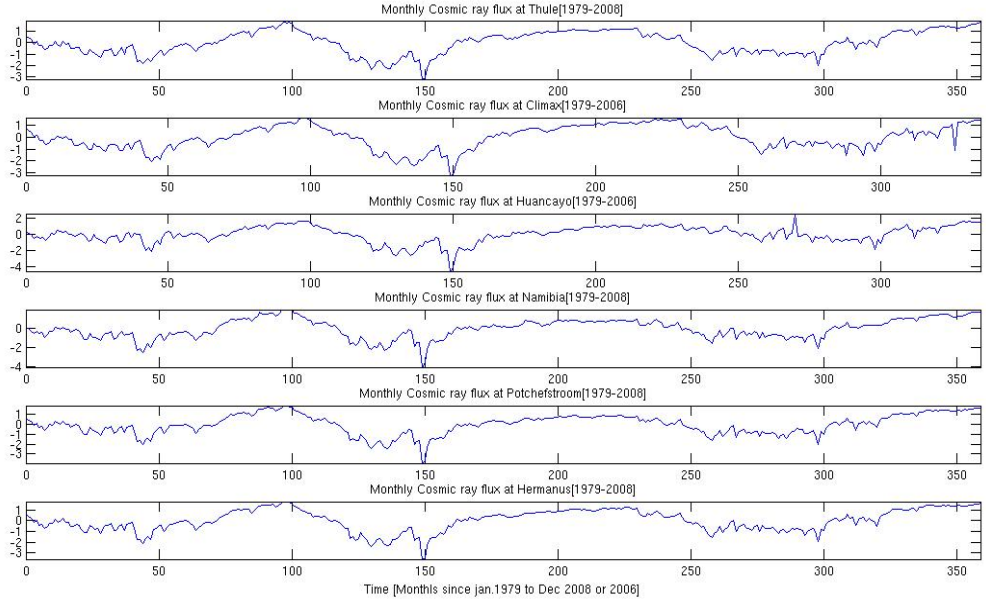

Figure 2.7: Normalized monthly Cosmic ray flux time series at six different locations. X-axis shows the time since 1979 in months. Y-axis represents the normalized cosmic ray flux amount. Due to unavailability of cosmic ray flux data after 2006 at Climax and Huancayo neutron monitor stations limits our analysis to a period of 28 years. However, at other four stations, the data has been plotted for a course of 30 years

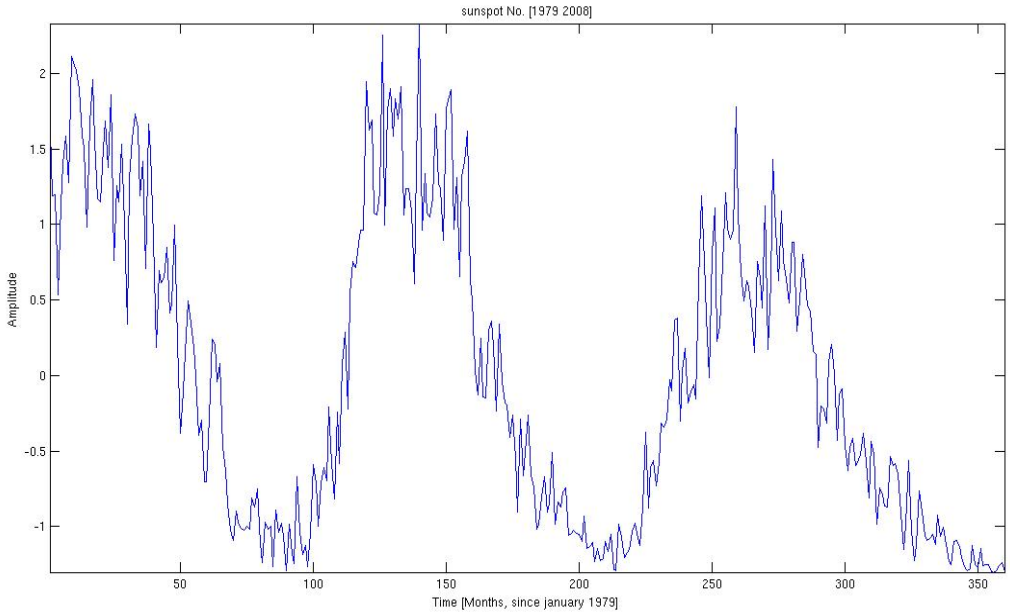

Figure 2.8: Normalized monthly sunspot number time series from 1979 to 2008. X-axis denotes the time in months since January 1979. Y-axis shows the number of sunspots during the time period

CHAPTER 3

TIME DOMAIN ANALYSIS

3.1 Introduction

In order to detect the possible relation between cloud cover or precipitation, with cosmic rays, we employ the correlation coefficient. This single parameter describes the strength of the relationship between two parameters. The method has been used intensively in bivariate statistics for possible connections between two variables.

3.2 Correlation Coefficient

Pearsons linear product-moment correlation coefficient is a measure of correlation or linear dependence between two variables. The values of the coefficient vary between $+1$ and -1. The sample correlation coefficient is used as a measure to determine the strength of the population's correlation. Mathematically, the sample correlation coefficient is defined as follows:

$$r_{xy} = \frac{\Sigma_{i=1}^{n}(x_i - \bar{x})(y_i - \bar{y})}{(n-1)\sigma_x\sigma_y} \tag{3.1}$$

where, n is the number of pairs of the data points x, y, σ_x, and σ_y represent the (sample) standard deviation of the time series $x(t)$ and $y(t)$ respectively, and $\bar{x}$ and $\bar{y}$ denote the mean values of the series.

The p-value is computed by transforming the correlation to create a so called t-statistic having *(n-2)* degrees of freedom, where n is the number of samples in our time series. Here $n(= 30)$ represents the number of years over which data is available when we use annual data. Basically, the p-value for a one tailed t-test is the probability that the absolute value of a point chosen at random from a particular t-distribution would be greater than or equal to the absolute value of an observed point (or t-value) from the same distribution. The formula involved in the computation of a p-value for Student's t-test is detailed below. The integral

of the Student t-distribution probability density function:

$$\frac{1}{\sqrt{\nu}\beta\left(\frac{1}{2},\frac{\nu}{2}\right)}\int_{t}^{-t}\left(1+\frac{x^2}{\nu}\right)^{\frac{-(\nu+1)}{2}}dx \tag{3.2}$$

where β is the beta function and ν is the number of degrees of freedom[1]. ($P < 0.05$ ($= \frac{1}{20}$) indicate that the probability of getting the correlation value by chance is 1 out of 20. Thus, the smaller is the p-value, lesser is the probability of getting the answer by chance and higher is our confidence in the result).
In the following subsections, the method is applied to test the strength of the correlation between cosmic ray flux, sunspot number, precipitation and low level cloud cover.

3.2.1 Correlation Coefficient between Solar Activity and Cosmic Ray Flux

We first consider two major parameters whose possible influence to the atmosphere we wish to assess, namely solar activity and the cosmic ray flux. To test the connection between the two variables we employ the method of correlation coefficient.

The table below displays the correlation coefficient between solar activity, here determined by the Wolf sunspot number, and the cosmic ray flux, measured in neutron counts. The annual sunspot and cosmic ray flux data have been considered for a period of thirty years, from 1979 to 2008. The thirty data points are normalized before computing the correlation coefficients.

From Table(3.1) we observe significantly high negative correlation between sun spot number and the cosmic rays. Moreover, the negative correlation between the neutron count and solar activity weakly increases with latitude, which may be accounted for by the geomagnetic cut-off rigidity factor, which is higher at the equator and decreases towards the poles. The lower geomagnetic cut-off rigidity at the poles allows a higher cosmic ray intensity to penetrate through the atmosphere

[1]Student, William Sealy Gosset (1908), Biometrika "The probable error of a mean", vol. 6(1), pp. $1-25$
Fisher, R.A. (1925), "Applications of Student's distribution", Metron, vol. 5,pp.90 to 104
Abramowitz, M and Stegun, I.A., eds.(1965), "Handbook of Mathematical Functions", Dover, New York, NY

Station	Latitude	Correlation Coefficient
Thule	76.5 N	-0.8267
Climax	37.37 N	-0.8076
Huancayo	12.03 S	-0.7736
Namibia	19.12 S	-0.8118
Potchefstroom	26.41S	-0.8219
Hermanus	34.25 S	-0.8361

Table 3.1: Table illustrating the Correlation Coefficient, above 99.9% significance level, between the sun spot number and the cosmic rays data at six stations

at higher latitudes. It may also be noted that the correlation coefficients are above 99.9% significance level.

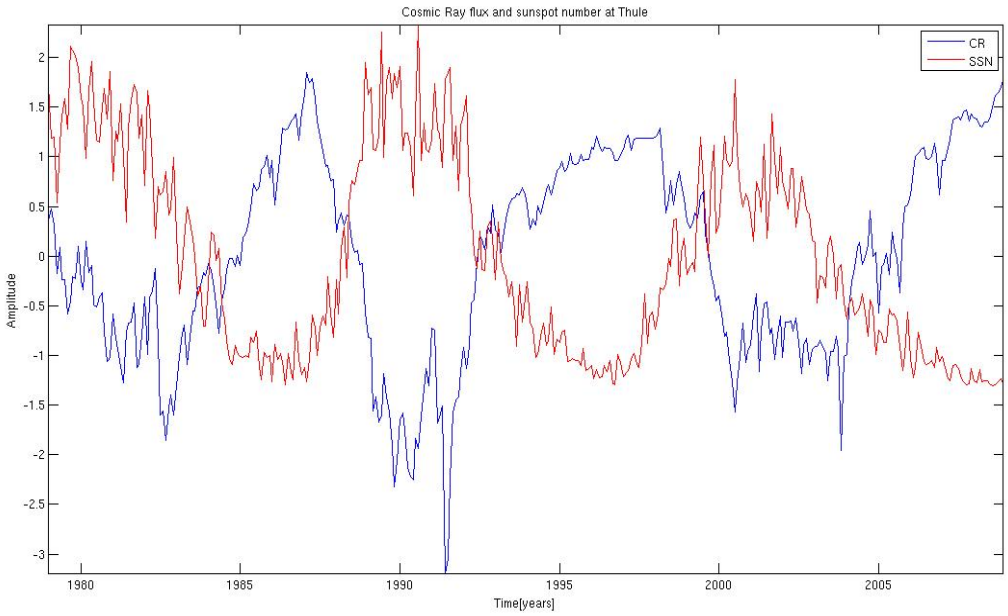

Figure 3.1: Standardized Cosmic ray flux and sunspot time series illustrating the negative association between them

3.2.2 Correlation Coefficient between the Cosmic Ray Flux and Low Cloud Cover

Next, we test the relation between the cosmic ray intensity and low cloud cover. This was proposed by Nigel Marsh and Henrik Svensmark[2] who have produced significantly high values of correlation for data from July 1983 to September 1994, obtained from International Satellite Cloud Climatology Project (ISCCP), New Cloud Datasets. We use the low cloud data, taken from ISCCP, new cloud datasets, and the cosmic ray flux at the six selected stations. However, as listed here in table(3.2) we could not find a significant correlation between the two parameters during the considered course of time. This can be due to the small sample size. The correlation coefficients and the p-values, along with the considered periods, are shown in Table (3.2) below.

Station	Correlation Coefficient	p-value	Duration
Thule	0.0275	0.7238	1994 to 2007
Climax	0.0135	0.8495	1994 to 2007
Huancayo	0.0033	0.9072	1994 to 2007
Namibia	-0.0376	0.6287	1994 to 2007
Potchefstroom	0.0193	0.8073	1994 to 2007
Hermanus	-0.0322	0.6785	1994 to 2007

Table 3.2: Correlation Coefficient, and corresponding p-values and (indicating varying significance level), between the low-cloud cover and the Cosmic Ray flux data at six stations during the time interval, Jan1994 to Dec2007

Conclusion

Thus during the period of 14 years (1994 to 2007), we have not found any significant correlation between low-cloud cover and the cosmic ray flux at any of the six stations. The considered time includes little more than a schewabe cycle, solar cycle of 11 years. Thus, the absence of any correlation can be accounted due to the short duration of data. Moreover, Svensmark claimed in his paper that the loss of correlation after September 1994 is due to a calibration problem of the

[2]H Svensmark, E. Friis-Christensen, Journal of Atmospheric and Solar, 1997, "Variation of cosmic ray flux and global cloud coverage– a missing link in solar climate relationships"

ISCCP satellites. In that case, even if the relation exists, we can not detect it without getting the correct data. Thus, we moved further to another important atmospheric variable, precipitation.

3.2.3 Correlation Coefficient between the Cosmic Ray Flux and Precipitation

The table(3.3) presents the correlation coefficients in the first column, the corresponding p-values in the next column and the period of the datasets in the third.

Station	Correlation Coefficient	p-value	Duration	Latitude
Thule	0.4633	0.0099	1979 to 2008	76.5 N
Climax	0.2583	0.1844	1979 to 2006	39.37 N
Huancayo	-0.0772	0.7020	1979 to 2006	12.03 S
Namibia	0.1558	0.4110	1979 to 2008	19.12 S
Potchefstroom	0.1071	0.5733	1979 to 2008	26.41 S
Hermanus	0.1594	0.4002	1979 to 2008	34.25 S

Table 3.3: Table furnish details about the correlation coefficient and the corresponding p-value between precipitation and cosmic ray intensity data at six stations
The correlation coefficient is significantly high at Thule neutron monitor station

From the table(3.3) we notice a highly significant correlation between cosmic ray intensity and precipitation at the Thule neutron monitor station. The probability of getting this correlation by chance is 1 out of 100.

Figure (3.2)illustrates the influence of geomagnetic cut-off rigidity, which decreases as latitude increases towards the poles. The positive connection between the cosmic ray intensity and precipitation rises with increasing latitude

3.2.4 Conclusion

The table(3.3) shows a gradual decline in the association between the cosmic ray flux and precipitation with decreasing latitude. And correlation between the CRF and precipitation is small and insignificant in the tropics. It has been shown that

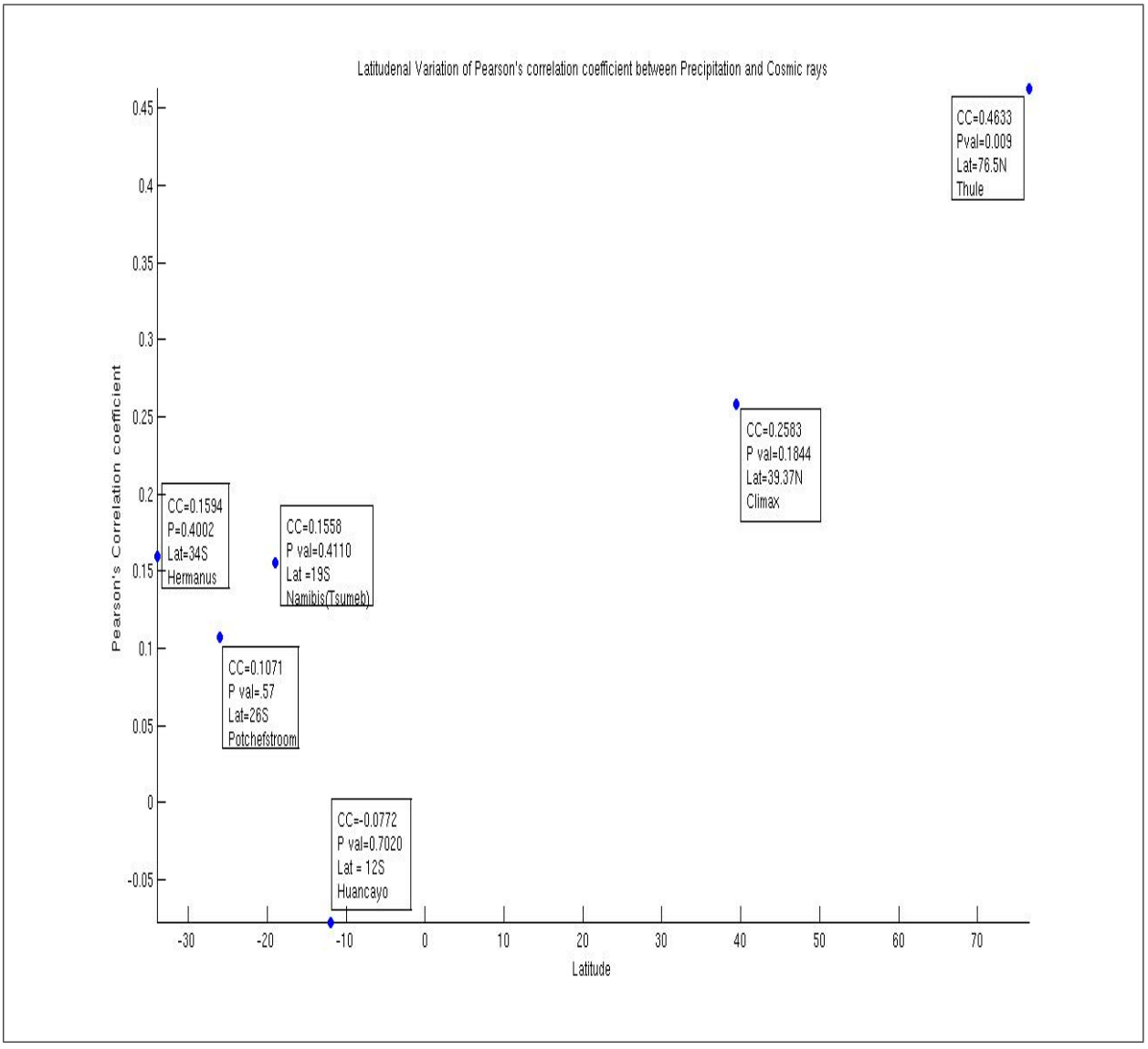

Figure 3.2: Variation of the association between cosmic ray flux and precipitation time series with Latitude

the solar activity influences rainfall in tropics[3].

From the table(3.3) we can infer that there is an absence of any signficant correlation at Huancayo.

3.2.5 Correlation Coefficient between the Sun Spot Number and Precipitation

In the previous section, we observed a negative connection, although insignificant, between the cosmic ray flux and precipitation in a tropical region called Huancayo. To investigate the result in detail, we look at the other side of the same coin. Here we perform the method of Pearson's correlation coefficient to detect any correlation of the sun spot number with the precipitation in the tropics. From table(3.4), we

Station	Correlation Coefficient	P-value
Thule	-0.5158	0.0009
Climax	-0.3846	0.0433
Huancayo	0.0580	0.7739
Namibia	-0.0800	0.6744
Potchefstroom	-0.0162	0.9324
Hermanus	-0.1864	0.3239

Table 3.4: Correlation coefficient and corresponding p-values between precipitation and the sun spot data at six stations

can infer that the precipitation at Thule and Climax neutron monitor stations is significantly anti-correlated to the sunspot numbers. At other stations, less significant anti-correlation can be noticed with an exception to Huancayo where the precipitation is positively correlated to the sunspot number but not quite significant. A moderate increase in the anti-correlation between the sunspot and precipitation,

[3]R Ananthakrishnan, B Parthasarathy - J. climatol, 1984 "existence of a weak positive association between Indian rainfall and sunspots" ;JC Stager, A.Ruzmaikin, D.Conway, P.Verburg, Journal of Geophysical, 2007 suggests that "Although irradiance fluctuations associated with the sunspot cycle are weak, their effects on tropical rainfall could be amplified by SST and ENSO ";MG Yadava, R Ramesh - New Astronomy, 2007 suggests that"A 12.5 to 13 year periodicity in climatic variability due to coupled tropical ocean atmosphere are most likely due to climatic system and unlikely due to solar sunspot cycle" (Moore et. al). FFT analysis of Indian monsoon rainfall (Hiremath and Mandi, 2004),Subarna bhattacharyya(2005) titled, "A wavelet analysis between solar processes, Indian monsoon rainfall and ENSO inices"

with the increase in latitude can be observed from table(3.4). Namibia again adds an exception with the anti-correlation value of 0.080, which is about 30 higher than that at Potchefstroom. Nevertheless, as the p-value at Potchefstroom is quite high, the correlation value is not significantly acceptable. On the contrary, the p-value at Thule and Climax are quite low thereby agreeing with the precipitation and cosmic ray flux association, therefore more sophisticated mathematical techniques are employed in the following chapters to analyse the cosmic ray and precipitation association hypothesis.

3.3 In a Nutshell

- Cosmic ray flux has been found to be anti-correlated with the sunspot number,*i.e* higher the solar activity, lower is the cosmic rays penetrating through the earth's atmosphere and vice-versa. This is observed at all the six locations. The negative relation apparently increases with the latitude, perhaps due to higher cut off rigidity or geomagnetic activity at the equator. Thus, polar regions or higher latitudes, beyond approximately 55 °, show greater correlation between cosmic ray flux and precipitation in the region.

- Insignificant but positive correlation coefficient between low cloud cover and cosmic ray intensity is found at 4 stations out of 6. However, Hermanus and Namibia in southern hemisphere show negative relation and hence present an exceptions.

- A significantly positive correlation between cosmic ray intensity and precipitation at Thule shows that precipitation is strongly dependent on the cosmic ray flux at that station. At the other 5 neutron monitor stations, the association between cosmic ray flux and precipitation is not significant, but positively correlated with an exception at Huancayo where the relation is negative.

- A small positive correlation, 0.06, between the precipitation and sunspot number was seen in the case of Huancayo. Thus, based on correlation analysis, in equatorial regions, solar activity seems to have weak or no effect on precipitation. This is in contrast to the poles where cosmic activity is more compelling.

CHAPTER 4

POWER SPECTRUM ANALYSES

4.1 Introduction

Over the course of 30 years, 1979-2008, precipitation and cosmic ray flux parameters showed strong correlation at the geographic poles, which may be accounted for by the deflecting effect of the geomagnetic field on charged particles, Chapter(1). Taking this fact into account, we now apply the power spectral density method to seek any significant periodicities present in the signals. Here, we have analysed two and a half Schwabe solar cycles. In the section to follow we first introduce the power spectral density method applied to the three time series, along with the Blackman-Tukey method and its modification using Welch-spectral analysis.

4.2 Analysing Techniques

4.2.1 Power spectral density (PSD)

Power spectral density (PSD) describes the way the power of the signal is distributed with frequency. Power spectral density like energy spectral density requires that the function to be analysed be *square integrable*[1] or the time series should be *square summable*[2]. However, few natural signals are not square integrable or square summable. But, if the signal or the time series is a stationary random process in the wide-sense, then the Wiener-Khinchin theorem provides a rigorous approach. A wide-sense stationary process is an approximately stationary process whose joint probability distribution does not change when shifted in time and space. In stochastic or random processes, there is some indeterminacy in their future evolution, described by a probability distribution, even if initial conditions are known. There are many possible paths that the process might take, but some

[1] a function whose square has a finite integral
[2] a series whose square has a finite sum

may be more probable than others. The PSD is then the Fourier transform of the auto-correlation function, $R(\tau)$, of the signal *i.e.*

$$\mathbf{PSD} = \int_{-\infty}^{\infty} R(\tau) \exp(-2\pi i f \tau) d\tau \tag{4.1}$$

The power of the signal in a given frequency band can be calculated by integrating over positive and negative frequencies in the band. The signal should be nearly stationary for the WienerKhinchin theorem to be applicable. If the process is non-stationary, the auto-correlation function would be a function of two variables and no power spectral density will exist. However, a similar technique to estimate a time-varying spectral density also exists[3].

4.2.2 Auto Spectral Analysis

Auto spectral analysis aims to describe the distribution of the variance of the signal with frequency (or wavelength). Autocovariance describes the variance of the time series over a time lag k. An unbiased estimator of auto-covariance of a signal, say $x(t)$, with N data points sampled at a constant time interval, say Δt, is given by:

$$Cov_{xx} = \frac{1}{N-k-1} \Sigma_{i=1}^{N-k} (x_i - \bar{x})(x_{i+k} - \bar{x}) \tag{4.2}$$

Autocorrelation of a data series refers to its correlation with itself, depending upon the time lag k. To obtain autocorrelation, the covariance cov_{xx} is normalized by the variance of the time series.

$$Corr_{xx} = \frac{Cov_{xx}(k)}{\sigma_x^2} \tag{4.3}$$

auto-correlation coefficient ($0 \leq \alpha \leq 1$). Here, we use the Welch technique with rectangular window to estimate the power spectrum of the stated variables. The basic idea behind this technique is the use of averaged periodogram of overlapped, windowed segments of a time series. The method reduces the variance associated

[3]Robert Grover Brown and Patrick Y.C. Hwang (1997). Introduction to Random Signals and Applied Kalman Filtering. John Wiley and Sons ISBN 0471128392. An Introduction to the Theory of Random Signals and Noise, Wilbur B. Davenport and Willian L. Root, IEEE Press, New York, 1987, ISBN 0-87942-235-1

with the standard periodogram by cutting the data into blocks and then averaging over their periodograms. Peaks in the spectrum are statistically tested against a classical statistical model of a first-order auto-regressive (AR1) process. The AR1 process(Y(t)) can be expressed by the equation:

$$Y(t) = \beta Y(t-1) + \epsilon(t), \tag{4.4}$$

where $\epsilon(t)$ is the white noise with zero mean and variance, σ_ϵ^2
β is the lag-1 auto-correlation coefficient ($0 \leq \beta < 1$).

The reference or control normalized power spectral density function for AR1 is given by:

$$P_k = \frac{1-\beta^2}{1+\beta^2-2\beta\cos(2\pi k/N)}^4 \tag{4.5}$$

where the frequency index k = 0, 1 , 2,. . . ,N/2 and the discrete time in units of the sampling interval is given, t=1,2,....,N. Lag-1 auto-correlation coefficient, β, determines the shape of the normalized power spectrum density function, P_k. Now, if β is greater than 0, the power is clustered at lower frequencies which is defined as the red noise spectrum. While, β less than 0 represents the concentration of the power at higher frequencies, which is known as the blue noise spectrum. However, if the value of β is 0 we get the spectrum with an average of one at all frequencies and the spectrum is called the white noise spectrum. The peaks are checked against the reference spectrum as described by equation(4.5).

The spectral peaks lying above the mentioned reference spectra are then subjected to χ^2 - test, with number of degrees of freedom equal to 2, and with a specific confidence level to check against the hypothesis that the peaks are part of the statistical fluctuations. If the time series is a normally distributed random variable then both the real and imaginary parts of its fourier spectrum are normally distributed too. Since the square of the normally distributed variable is chi-square distributed with 1 degree of freedom, the complex power spectrum is chi square distributed with two degrees of freedom. In order to determine say 99% confidence level,(significant at 1%), one multiplies the reference spectrum P_k by the 99^{th} percentile value for the χ^2 - distribution with 2 degrees of freedom and

[4]D. L. Gilman, F. J. Fuglister and J. J. Mitchell, J. Atmos. Sci. 1963, The power spectrum of Red noise, 20 (1963) 182184.

checks if the peaks lie above the 99^{th} percentile. The significance is tested against the background spectrum .

4.2.3 Spectral Analysis of Precipitation and Cosmic Ray Flux at Thule

As in figure (4.1,4.2), the auto-spectrum of the precipitation at Thule shows a dominant peak of 10 years corresponding to the frequency of 0.1 (cycles/year) while the other significant peaks of 3.3 and 2.7 years carry about 75% less power than the dominant peak of ten years. Auto-spectrum of the cosmic ray flux at Thule displays two major cycles. The one carrying the highest power is the 10 year cycle, and is above the 99% confidence level. The other cycle corresponding to 5 years is significant above the 95% confidence level.

4.2.4 Spectral Analysis of Precipitation and Cosmic Ray Flux at Climax

As can be seen in figure (4.3,4.4), the spectral peak of 0.43 cycles/year in precipitation time series can be distinguished clearly from other peaks in the graph, which occur at a frequency of 0.067 cycles/year or a period of about 15 years. The other two dominant peaks of 6 and 2 years are significant above 95% confidence level.

The cosmic ray intensity at Climax is considered for a period of 28 years, from 1979 to 2006. The power peaked only at a 9.3 year cycle which is significant above 99% confidence level.

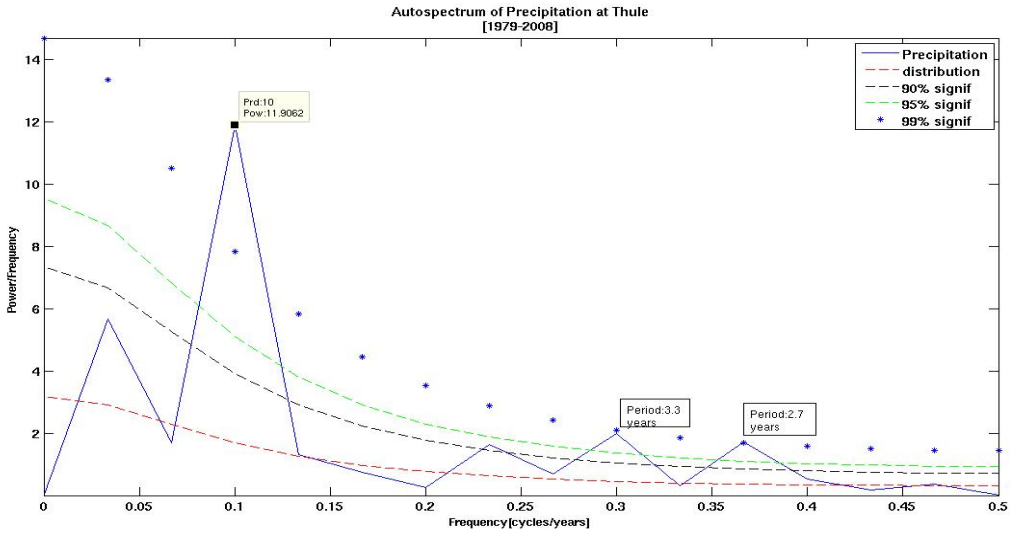

Figure 4.1: Power Spectrum of Annual Precipitation at Thule from 1979 to 2008. X-axis represents the frequency in cycles per year. Y-axis shows the power per unit frequency.

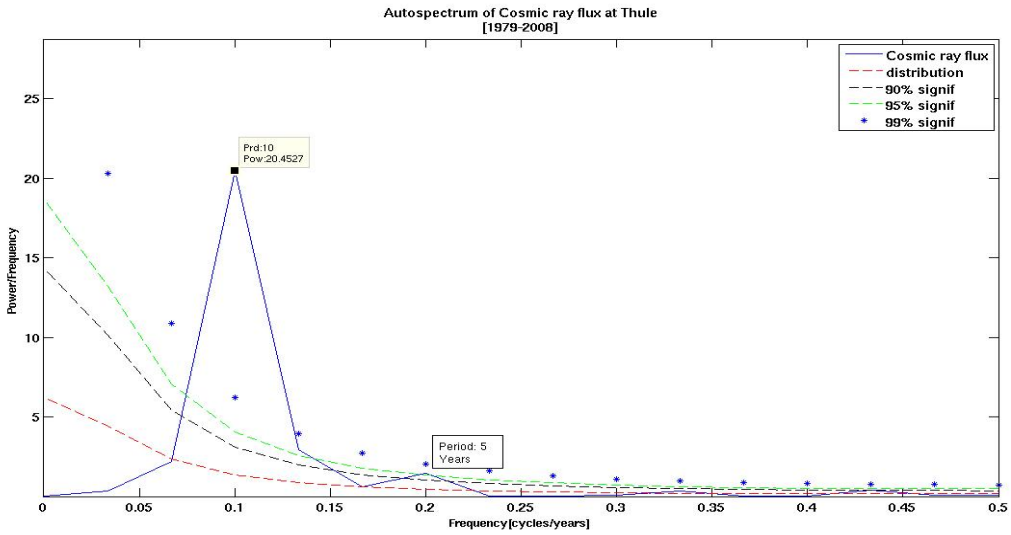

Figure 4.2: Power Spectrum of Annual Cosmic Rays at Thule from 1979 to 2008.X-axis represents the frequency in cycles per year. Y-axis shows the power per unit frequency.

4.2.5 Spectral Analysis of Precipitation and Cosmic Ray Flux at Huancayo

Figures(4.5, 4.6) show that the auto spectral graph of the precipitation at Huancayo reveals several peaks, the most dominant being at 4.3 years, corresponding to the

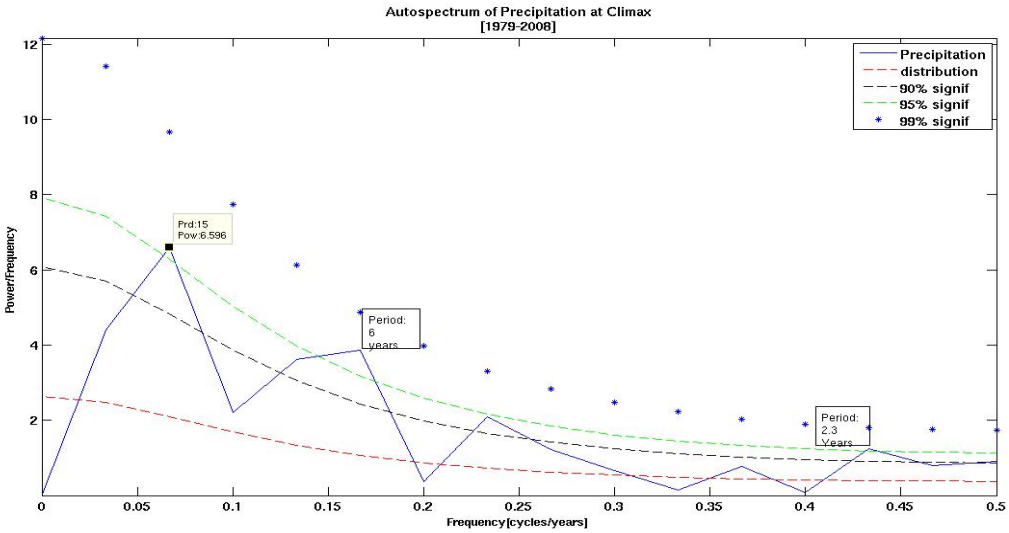

Figure 4.3: Power spectrum of annual precipitation at Climax from 1979 to 2008.X-axis represents the frequency in cycles per year. Y-axis shows the power per unit frequency.

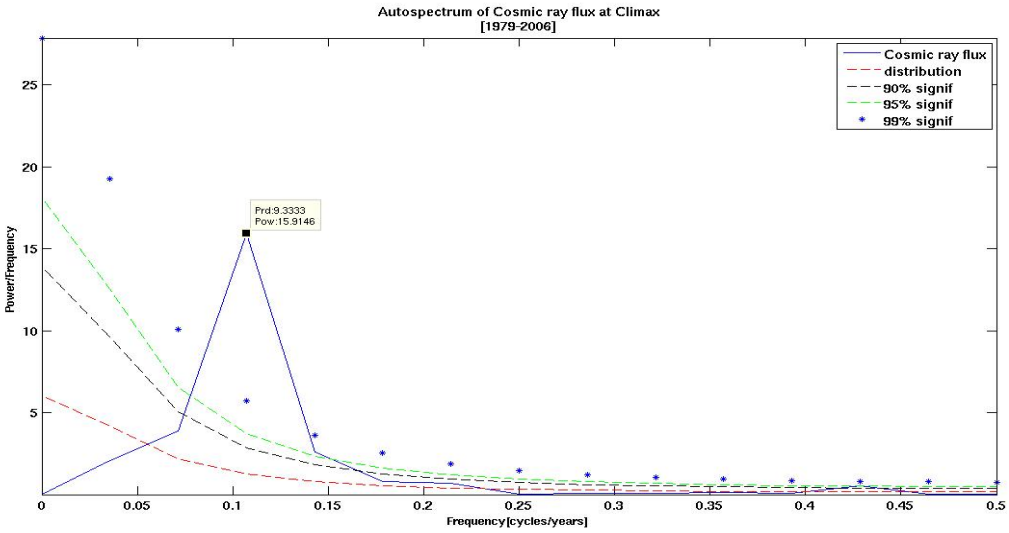

Figure 4.4: Power Spectrum of Annual cosmic rays at Climax from 1979 to 2006.X-axis represents the frequency in cycles per year. Y-axis shows the power per unit frequency.

frequency of 0.233 (cycles/year) and significant above 99% confidence level. The three most significant peaks correspond to 15, 2.5 and 4.3 years, which together carry approximately 31% less power than the dominant peak of 4.3 years.

The neutron monitor count at *Huancayo* for the period 1979 to 2005 shows a 9 year cycle above 99% confidence interval.

4.2.6 Spectral Analysis of Precipitation and Cosmic Ray Flux at Namibia

The power spectrum for precipitation at Namibia shows interesting features. As in the figure(4.7,4.8), the primary cycle of 3 years is above 99% confidence interval. The longer period of 10 years is above 95% confidence level and carries 69% less power than that of the 3 year cycle.

At Namibia the periodogram reveals one distinguishable cycle of 10 years which is above 99% confidence level.

4.2.7 Spectral Analysis of Precipitation and Cosmic Ray flux at Potchefstroom

A distinct 10 year cycle in precipitation time series is above 99% confidence level. Apart from the major 10 year cycle, there are 5, 2 and 2.5 year cycles above 95% confidence level. The auto-spectrum of cosmic rays at Potchefstroom, figure(4.9, 4.10), for a data set spanning three decades, from 1979 to 2008, reveals one predominant period. The dominant peak of 10 years, above 99% confidence interval.

4.2.8 Spectral Analysis of Precipitation and Cosmic Ray Flux at Hermanus

From figures(4.11, 4.12), the power spectrum of annual precipitation at Hermanus for a period of three decades, beginning from January 1979 and ending in December 2008, illustrates diverse periods. A 3 year cycle is the dominant period, at above 99% confidence level. However, a longer period of 10 years is significantly high above 95% confidence interval. 10 year and 2.3 year cycles are present in the

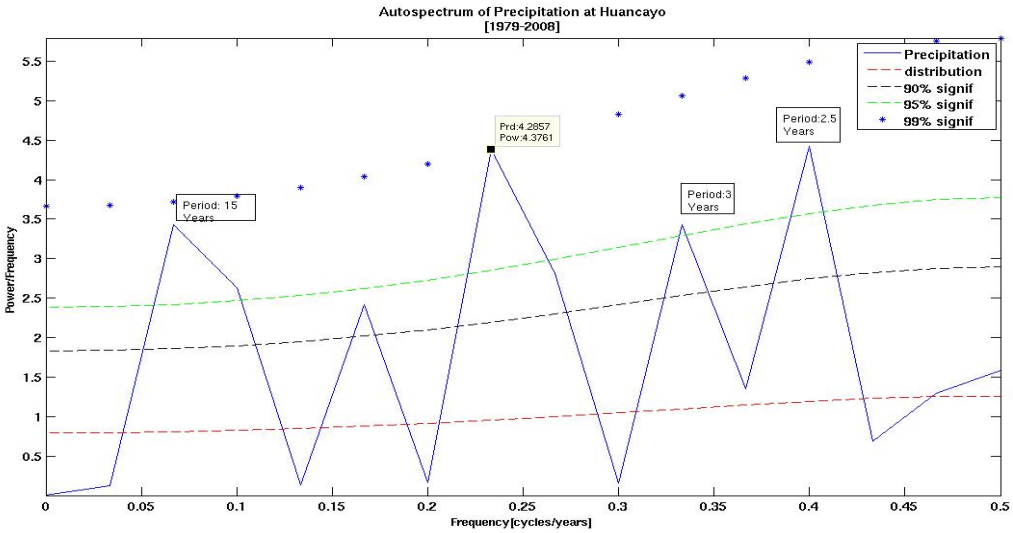

Figure 4.5: Power spectrum of annual precipitation and Cosmic Rays flux at Namibia from 1979 to 2008.X-axis represents the frequency in cycles per year. Y-axis shows the power per unit frequency.

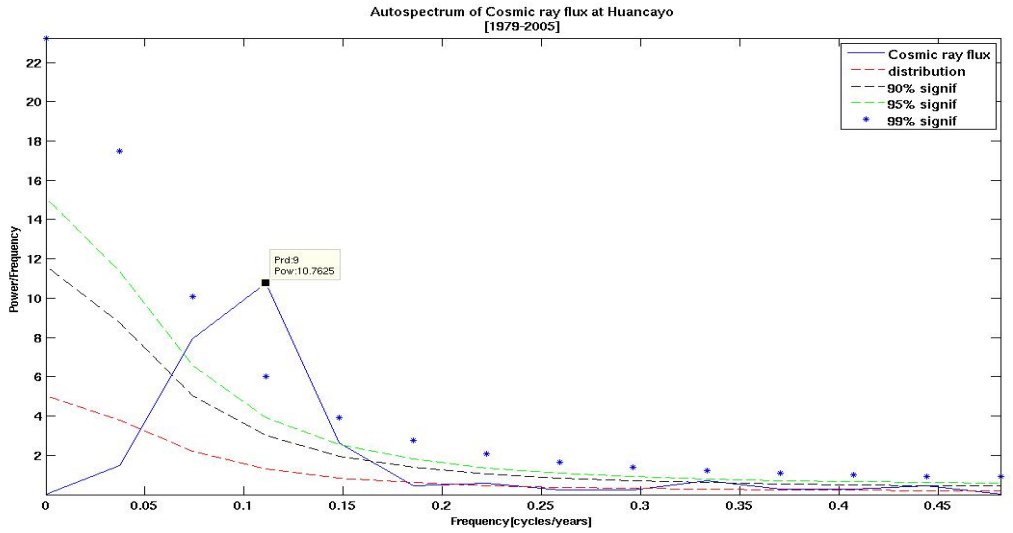

Figure 4.6: Power spectrum of annual cosmic rays at Huancayo from 1979 to 2008.X-axis represents the frequency in cycles per year. Y-axis shows the power per unit frequency.

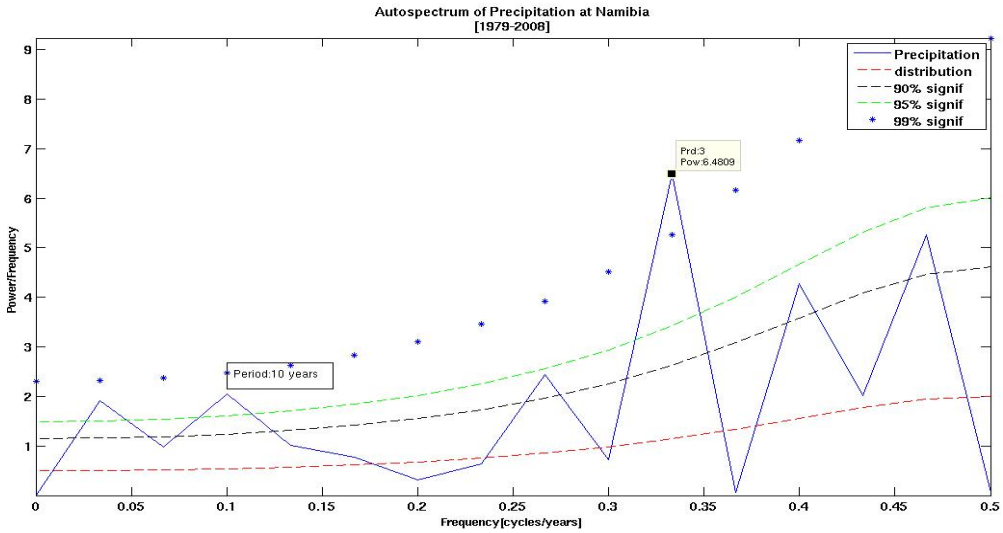

Figure 4.7: Power spectrum of annual precipitation at Namibia from 1979 to 2008.X-axis represents the frequency in cycles per year. Y-axis shows the power per unit frequency.

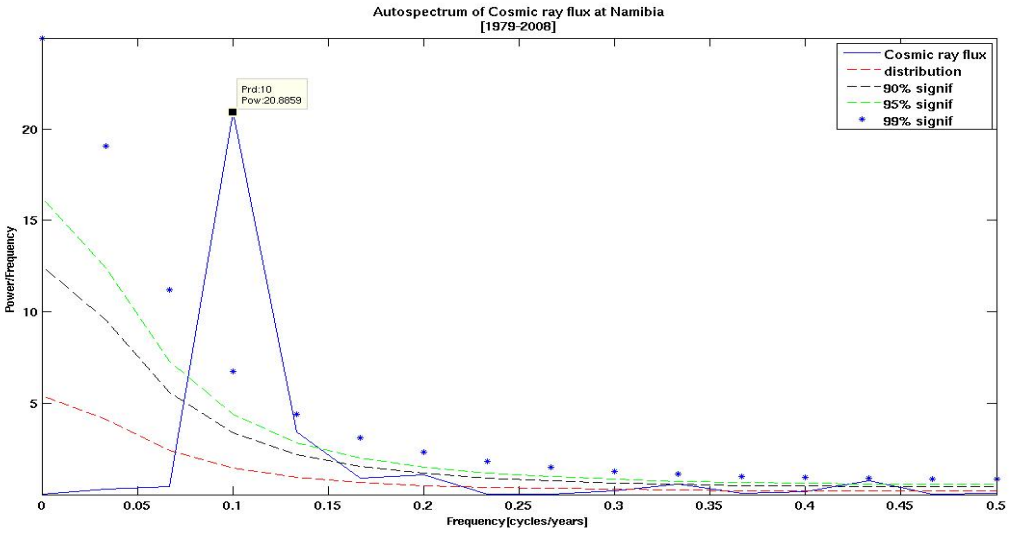

Figure 4.8: Power spectrum of annual cosmic Rays at Namibia from 1979 to 2008.X-axis represents the frequency in cycles per year. Y-axis shows the power per unit frequency.

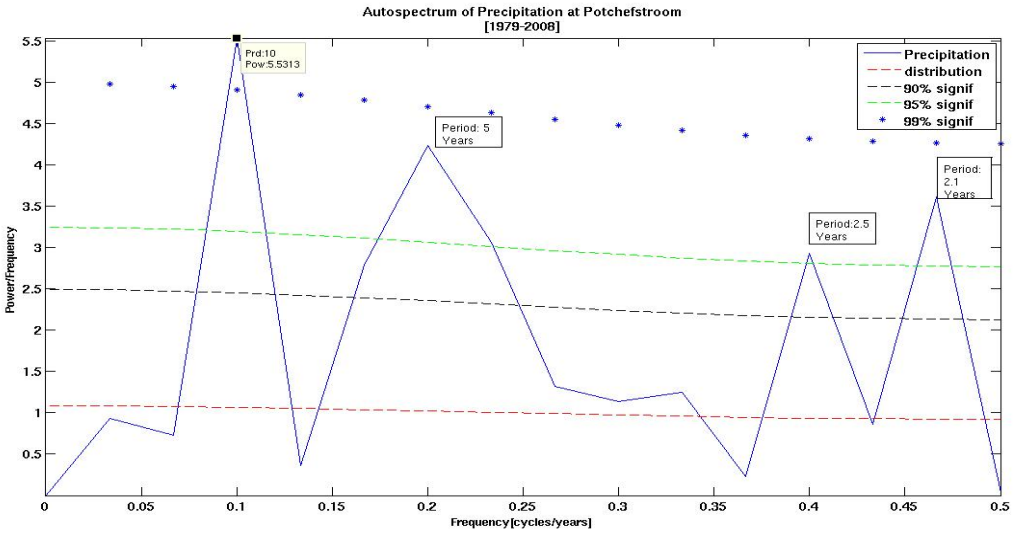

Figure 4.9: Power spectrum of annual precipitation at Potchefstroom from 1979 to 2008.X-axis represents the frequency in cycles per year. Y-axis shows the power per unit frequency.

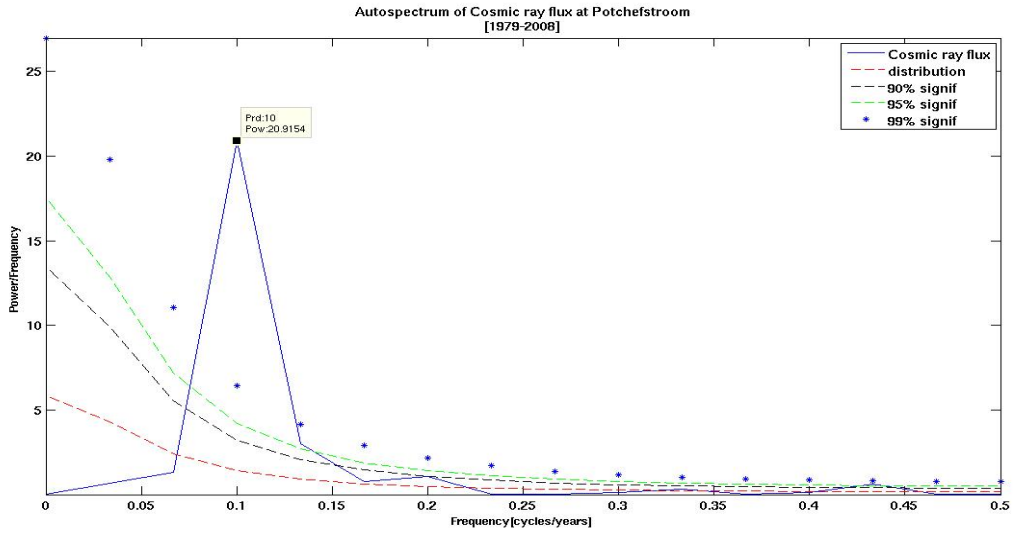

Figure 4.10: Power spectrum of annual cosmic rays at Potchefstroom from 1979 to 2008.X-axis represents the frequency in cycles per year. Y-axis shows the power per unit frequency.

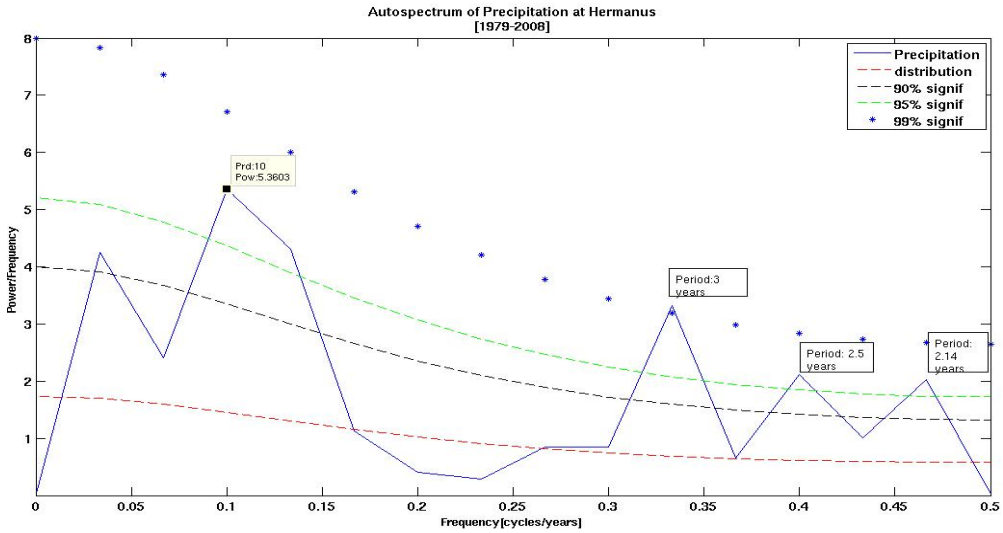

Figure 4.11: Power spectrum of annual precipitation at Hermanus from 1979 to 2008.X-axis represents the frequency in cycles per year. Y-axis shows the power per unit frequency.

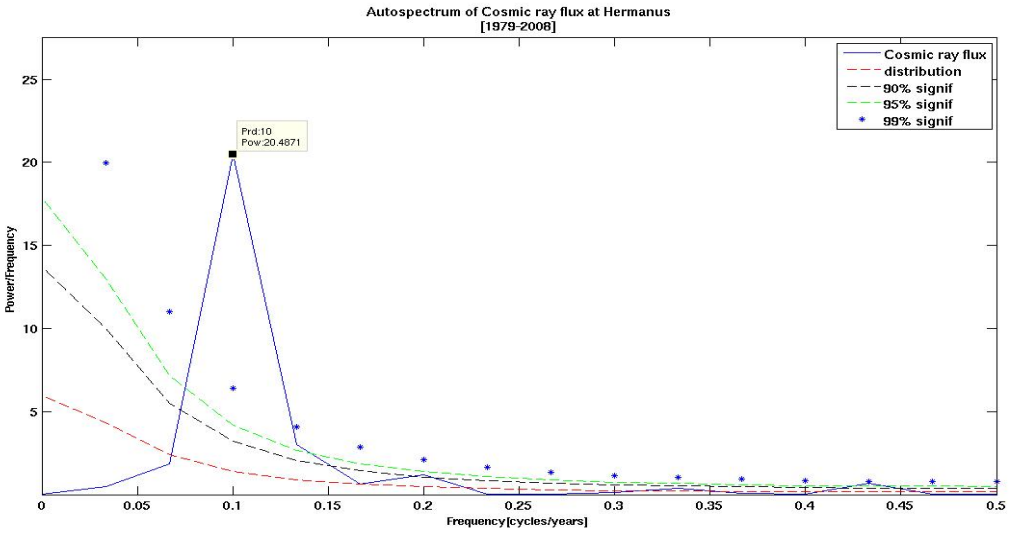

Figure 4.12: Power spectrum of annual cosmic ray flux at Hermanus from 1979 to 2008.X-axis represents the frequency in cycles per year. Y-axis shows the power per unit frequency.

auto spectrum of annual cosmic ray flux at Hermanus, where the former cycle is above 99% confidence level and the second cycle is significant above 95% confidence interval.

4.3 Solar Activity

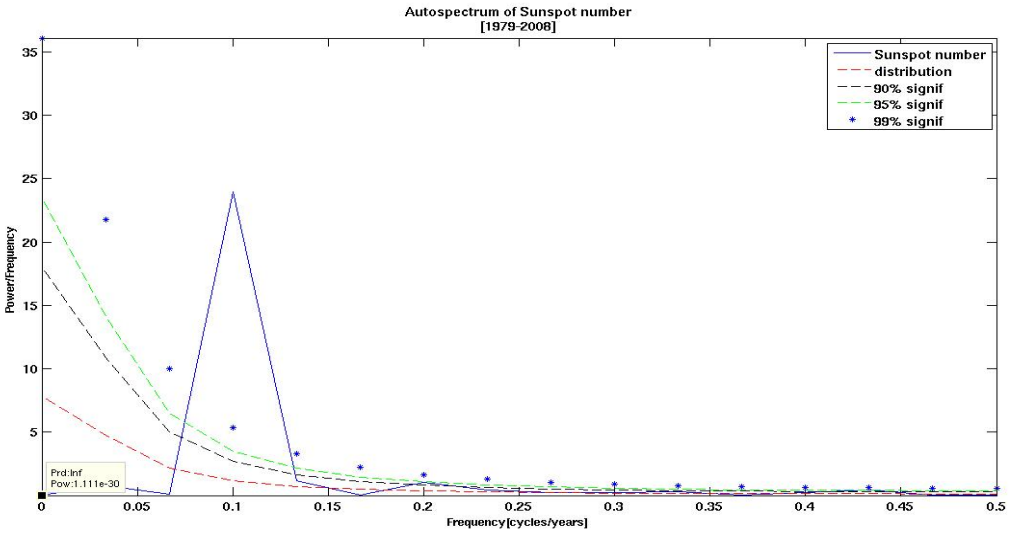

Figure 4.13: Power spectrum of annual solar activity, sunspot numbers for a period of three decades, from 1979 to 2008.X-axis represents the frequency in cycles per year. Y-axis shows the power per unit frequency.

As can be noticed from figure(4.13), a 10.8 year cycle is the dominant cycle in the spectrum of the sunspot number. This cycle is above 99% significance level. Apart from the 10.8 cycle, a 5.5 year cycle can be observed too.

4.4 Results and Conclusions

From Table (4.1), in the band of 10-11 years, dominant peaks are observed in the precipitation as well as the cosmic ray flux time series at Thule. However, at Climax, Potchefstroom and Hermanus the significant cycle in the same band, above 99% confidence interval, is also present. As these time series are non-stationary in nature, wavelet spectral analysis is preferred over other methods and is applied in the following chapters. In table (4.2) Significant Schwabe cycle of about 11 years can be observed in the power spectrum of sunspot number during the period from 1953 to 2008. And a dominant cycle of 10 years can be noticed in the the sunspot number during the period from 1979 to 2008.

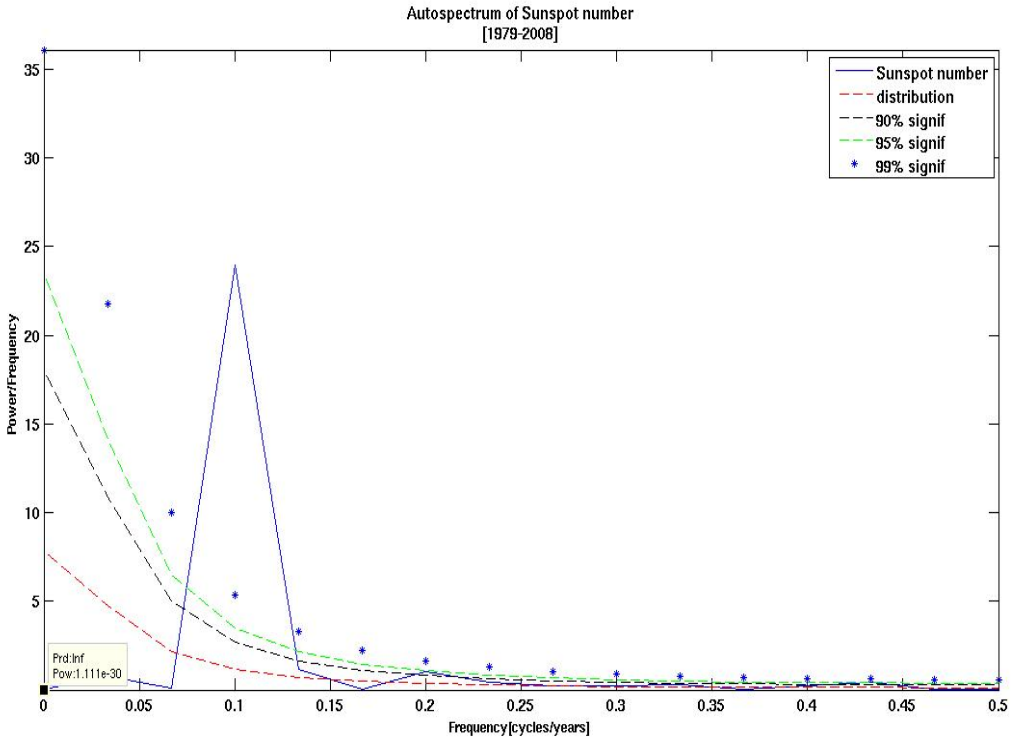

Figure 4.14: Power spectrum of annual solar activity, sunspot numbers for a period of three decades, from 1979 to 2008.X-axis represents the frequency in cycles per year. Y-axis shows the power per unit frequency.

Station	Cycles in cosmic ray flux	Cycles in precipitation
Thule	10(>99%),5(>95%)	10(>99%),3.3,2.7(>95%)
Climax	9.33(>99%)	15,6,2(> 95%)
Huancayo	9(>99%)	4.3(> 99%),15,2.5,3(> 95%)
Namibia	10(>99%)	3(> 99%),10(>95%)
Potchefstroom	10(>99%),2.3(>95%)	10(> 99%) 5,2.5,2(> 95%)
Hermanus	10(>99%),2.3(> 95%)	3(> 99%) 10(> 95%)

Table 4.1: List of cycles (in Years) in cosmic ray flux and precipitation at six stations from power spectrum analysis

4.5 In a Nutshell

The present power spectral statistical analysis uncovers several important periodic cycles as follows. It may be noted that the cycles are significant above 99.9%

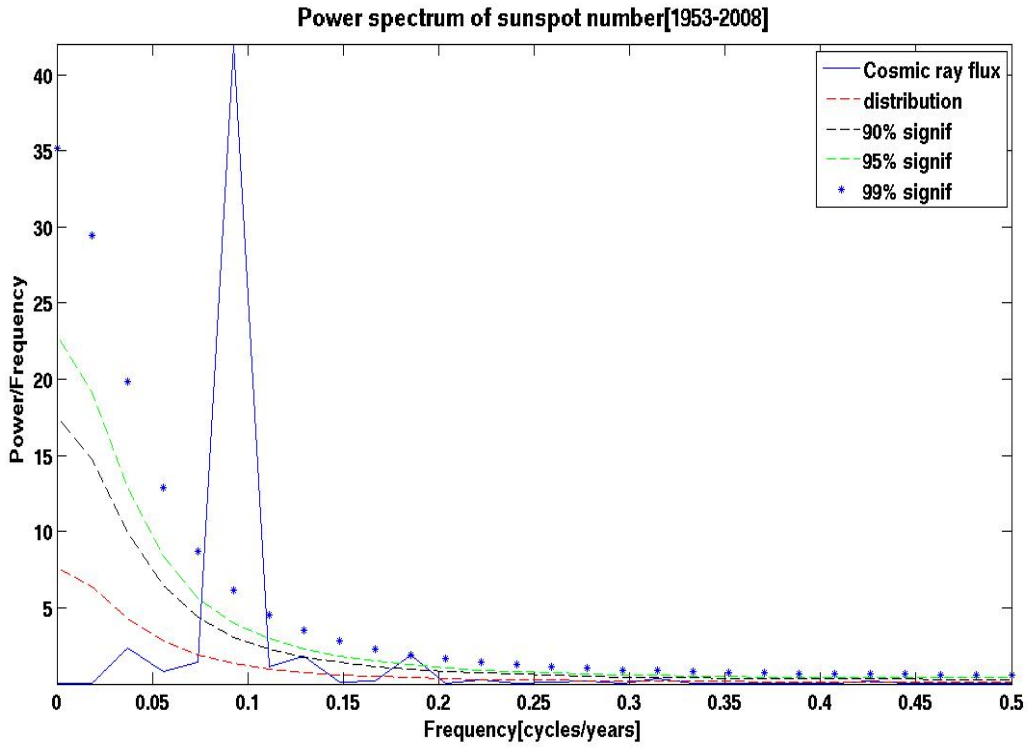

Figure 4.15: Power spectrum of annual sunspot numbers from 1953 to 2008.X-axis represents the frequency in cycles per year. Y-axis shows the power per unit frequency.

Cycles in sunspot number[Years]	Duration
10	1979 to 2008
10.8	1953 to 2006

Table 4.2: Cycles (in Years) in sunspot number using Auto power spectrum.

confidence interval, while considering red noise spectrum as the background noise.

- A cycle with a period of 10 years is noticed in the precipitation, and a period of 10.9 years duration in the case of cosmic ray flux at Thule.
- At Climax, cosmic rays as well as precipitation show a common cycle of 10 years.
- In the tropics, at Huancayo, a cycle of duration 4 years is highly significant

in the case of precipitation and a cycle of 10 years in the power spectrum of the cosmic rays.

- A periodicity of 10 years in the case of cosmic flux and 3 years, significant above 99percent significance level, in the power spectrum of precipitation at Namibia is observed.
- At Potchefstroom, a 10 year cycle and a 10.9 year cycle are present in the spectrum of the precipitation and cosmic ray flux respectively.
- Both precipitation as well as cosmic ray flux power spectrum at Hermanus illustrate a major cycle of 10.9 years and a secondary cycle of 7.05 years
- A cycle of 10.9 years is displayed in the power spectrum of solar activity.

Thus, a similar cycle of with an approximately 10 year period is recorded in the case of the cosmic ray parameter and the precipitation data at higher latitudes viz- Thule, Climax and Hermanus.

In the analysis we found dominant 10 and 10.9 year cycles present in the cosmic ray and sunspot power spectrum at all the six stations. However, these cycles are also present in the precipitation time series at four out of the six neutron monitor station viz- Thule, Climax, Potherstroom and Hermanus. The existence of a 10-year cycle in the precipitation time series at Thule and the periodicity of 10.9 years in the cosmic ray signal at that station provides motivation for further analysis. This can be done using advanced mathematical techniques, such as wavelet spectrum which is strongly recommended for a non-stationary time series.

CHAPTER 5

WAVELET POWER SPECTRUM

With the advent of new mathematical techniques, we have several analysing tools suited to different types of time series. To begin with, Fourier transform(FT) is a powerful tool to resolve a stationary time domain signal into its frequency components. However, it is not useful in analysing a non-stationary signal, whose statistical properties vary with time. Many natural signals like speech and music are non-stationary in nature. Thus a method called Short Time Fourier Transformation (STFT) was proposed to overcome the limitation of the Fourier Transformation. STFT is simply the FT of the function with a time varying window. The data is broken up into fragments, which generally overlap to reduce artifacts at the boundaries. Each part is then Fourier transformed and the complex result is added to a matrix, which records magnitude and phase for each instant in the time and frequency plane[1]. STFT is well known in speech processing. Despite its advantages, it should be noted that it uses a window of a fixed size that does not change with time, thus resulting in lower time resolution for non uniformly distributed signals like transient and discontinuous signals. To overcome the shortcoming of constant-size windows, a new advanced tool known as Wavelet Transformation was introduced. Wavelet transformation involves variable size windows and uses wavelet bases which are oscillatory, of limited duration, and possibly asymmetric in nature. These are in contrast to the traditional sine or cosine functions which were used as the basis functions in power spectrum analysis.

We have used the 'real morlet' wavelet for continuous wavelet transformation. The data considered at Thule, Namibia, Potchefstroom and Hermanus neutron monitor stations is over the period from, 1979 to 2008, which spans 30years , a time period between 1979-2006 at Cli-

[1]Wikipedia

max, which spans 28 years, and finally a data set for a period of 27 years from 1979 to 2005 at Huancayo. Through this analysis, we find that the global wavelet spectra of precipitation and cosmic rays at Thule shows a dominant common cycle of 10 years, thereby revealing the periodicity. Here, we briefly explain the wavelet technique taking an example. By looking at the considered time series plot one can not always discern the non-stationary nature of a time series. We begin by detecting the non-stationarities in the time series by applying the wavelet technique. Then, we calculate the power in a period band in which there is greatest power. In the later sections, using wavelet power spectrum and local scaling (which is employed for highlighting the dominant value of coefficients over each scale), we find similar periodicities in the cosmic ray flux and precipitation series at higher latitudes (e.g. Thule neutron monitor station).

5.1 Introduction

In this chapter, at each of the six selected stations and for each of the variables, we compute power in a particular period-band and then compare the percentage of power in different bands. This technique will help to probe the common bands if any in each of the variables, precipitation, cosmic ray flux and solar activity. The advantage of this method over previously mentioned techniques is that it will take into account the diffusive nature of the wavelets and will show if the periodicity in a particular range of time periods exists. If the cycles occur in the same period band, then the two physical phenomena considered can be expected to have a reasonable connection, as one is inducing the other. For instance, the cosmic rays being highly charged and energetic particles, ionize the atmospheric gases nitrogen and oxygen, which then act as condensation nuclei. This enhances cloud formation which results in precipitation at appropriate conditions of temperature and pressure. But the mechanism of ionization followed by condensation which ultimately causes rainfall occurs over a period of time. Thus we expect a time lag between the two events, namely, ionization, caused by the impinging energetic particles, and the precipitation at appropriate temperature and pressure. The lag can be measured by finding the phase difference between the two phenomena, and

the method to find the phase lag/lead will be discussed in the next chapter. Here, we are seeking the common period bands that exist in different time series.

Wavelet transformation, which is a transform from one dimension(time or frequency) to two dimensions(time-frequency image), has been applied to the precipitation, cosmic ray flux and solar activity time series to make a quantitative comparison of the wavelet power over the dyadic period bands: 2-4, 4-8, 8-16, 16-32 years. The percentage of total wavelet power for each dyadic period band is computed and illustrated in several different plots at different geographic latitudes.

5.2 Brief Introduction to Wavelets

Mathematically, a wavelet transformation decomposes a signal $y(t)$ into some elementary functions $\psi_{a,b}(t)$ derived from a mother wavelet $\psi(t)$ by dilation, a, and translation, b :

$$\psi_{a,b}(t) = \frac{1}{\sqrt{a}}\psi\left(\frac{t-b}{a}\right) \tag{5.1}$$

here the mother wavelet, ψ, the translation is $a(>0)$, and the scale or the dilation of the wavelet[2] is called the daughter wavelet. The convolution integral of the mother wavelet $\psi(t)$with the signal $y(t)$ gives the wavelet transform of the signal, which is given by

$$W(b,a) = \frac{1}{\sqrt{a}}\int \psi^*\left(\frac{t-b}{a}\right)y(t)dt \tag{5.2}$$

where ψ^* is the complex conjugate of the mother wavelet, ψ

5.2.1 Characteristics of mother wavelets:

1. It should have zero mean,

$$\int_{-\infty}^{\infty} \psi(t)dt = 0 \tag{5.3}$$

   This property implies that the function is oscillatory or has a wave-like appearance

[2]Lau and Weng 1995, "A practical guide to wavelet analysis: How to make time series sing"

2. The function should be square integrable *i.e.* it should have finite energy,

$$\int_{-\infty}^{\infty} \psi^2 dt < \infty \tag{5.4}$$

This property suggests that most of the energy is confined to a finite duration[3].

5.2.2 Types of Wavelets

A few examples of real wavelets are now given:

Haar : Haar wavelet is the simplest of all the wavelets and is a discontinuous wavelet. It resembles a step function, the same representation as Daubechies-1(db1) wavelet.

Daubechies(db) : The compactly supported orthogonal property of the wavelet makes it suitable for discrete wavelet analysis. In MATLAB's wavelet toolbox, a comprehensive collection of routines for examining local, multiscale, and non-stationary phenomena has been provided. A variety of Daubechies wavelets available in the toolbox are, db1, db2, db3, db4, db5, db6, db7, db8, db9 and db10.

Biorthogonal : The Bi-orthogonal wavelet is one of the best known wavelets for signal and image reconstruction, because of its linear *phase property.*

Coiflets : This wavelet consists of two functions, namely, ψ and ϕ. The function ψ has $2N$-moments equal to 0 and the scaling function, ϕ has $(2N-1)$ moments equal to 0. The two functions have a support of length, $(6N-1)$. It is more symmetrical than the db wavelet.

Symlets : This is a nearly symmetrical wavelet and shares similar properties with the db wavelet. The Symlet wavelet was proposed by Daubechies.

Morlet : The real morlet wavelet has no scaling function, but is explicit.

Mexican Hat: Like morlet this wavelet has no scaling function and is derived from a function that is proportional to the second derivative of the Gaussian distribution.

Meyer: This function and the scaling function are defined in the frequency domain.

[3]Raghubeer M. Rao and Ajit S.Bopardikar, "Wavelet transforms"

Complex Wavelets :A few complex wavelet families available in the MATLAB's wavelet toolbox are described briefly below.

1. *Complex Gaussian wavelet:* Starting from the complex Gaussian function, $f(x)$, which is given as

$$f(x) = C_p \exp(-ix) \exp(-x^2), \tag{5.5}$$

the p^{th} derivative of $f(x)$, $\frac{d^p f(x)}{dx^p}$ is taken where p is an integer parameter of the wavelet family.

2. *Complex Morlet wavelet:* Complex morlet wavelet depends upon two parameters, f_c and f_b. Where f_c is a central frequency of the wavelet and f_b is a band width parameter.

$$\psi(x) = \frac{1}{\sqrt{\pi f_b}} \exp(2\pi i f_c x) \exp(-x^2/f_b) \tag{5.6}$$

3. *Complex frequency $B-Spline$ wavelet:* This wavelet is defined as:

$$\psi(x) = \sqrt{f_b}\left(sin\Big(\frac{f_b x}{m}\Big)\right)^m \exp\Big(2\pi i f_c x\Big), \tag{5.7}$$

This wavelet depends upon the three parameters, m f_b f_c. where, $m(\geq)$ is an integer order parameter,
f_b is a bandwidth parameter and
f_c is the wavelet central frequency

5.2.3 The Morlet Wavelet

The Morlet wavelet is the most popular wavelet in geo-sciences because of the explicit relation between the wavelet scale of the sequence and the standard fourier components. Thus a direct comparison between the discrete fourier transform components and wavelet transformation components can be made [4].

The complex morlet wavelet, which has been used for this study, is given by:

$$\psi_\circ(\eta) = \pi^{-1/4} \exp(i\omega_\circ(\eta)) \exp\left(\frac{\eta^2}{2}\right) \tag{5.8}$$

where, η is the non-dimensional time and $\omega_\circ$ is the angular frequency (in the time domain) of the oscillations within the wavelet itself.[5]

5.2.4 Method adopted to plot the wavelet power spectrum

MATLAB software has been used to compute the wavelet coefficients. The continuous wavelet transform coefficients have been plotted using contour plots to visualize the power spectrum of the data. The power spectrum is the absolute squared value of the wavelet coefficients for a real mother wavelet and absolute square for the complex wavelet, or the squared norm $|W(b,a)W(b,a)^*|$. A continuous wavelet transform divides a continuous time into wavelets and provides good time and frequency resolution.
The method involved in the analysis is explained step by step as follows:

Defining scales

The compression or dilation of the wavelet is defined by the size of the scale. For instance, smaller scales represent compression of the wavelet, while the larger scales correspond to dilation of the wavelet. The larger scales represent the lower frequencies and therefore have the capability to map the long-term variations in the time series. On the other hand, smaller scales correspond to the higher frequencies and hence can map rapidly-changing details.

[4]Reik V. Donner, Susana M. Barbosa, 2008, "Nonlinear time series analysis in the geosciences: Applications in climatology , geodynamics ans solar terrestrial physics"

[5]Torrence and Compo,1998, Bulletin of the American meteorological society "A practical guide to wavelet analysis"

Computing the wavelet coefficients

The coefficients are calculated using equation (5.2). Along with the wavelet coefficients, the corresponding scalogram which represents the percentage of energy for each coefficient is also calculated. The scalogram thus obtained is plotted. Using MATLAB wavelet toolbox for this purpose, we get a $l_a X l_s$ matrix, where la is the length of scales. Here, the contour representation of the scalogram is displayed.

5.3 Global Wavelet Power Spectral Analysis

The global wavelet power spectrum (GWPS) is an efficient estimator of the true measure of the power spectrum of the time series. Global wavelet power spectrum is the average over the time range and all the wavelet spectra. Mathematically, global wavelet power spectrum is given as follows:

$$\bar{W(s)}^2 = \frac{1}{N}\Sigma_{n=0}^{(N-1)}|W_n(s)|^2 \tag{5.9}$$

where N represents the length of the time series in, number of data samples. For instance, we have considered annual data for a duration of 30 years and each data point presents an annual value, thus N = 30. The symbol s denotes the scales in units of time (here year). Global wavelet power spectrum (GWPS) provides a useful measure of the background power spectrum, against which peaks in the local Global Wavelet Spectrum can be tested[6] As the Fourier spectrum is progressively smoothed, it approaches closer to the GWPS. However, the amount of necessary smoothing decreases with increasing scales.[7] The techniques have been applied to the normalized data.

5.3.1 Description of the wavelet power spectrum maps

The wavelet power spectrum maps shown here are the colour coded contour plots of the wavelet coefficients, derived from the wavelet transform of the signal. The

[6]D. Maraun , J. Kurths, 2004, Kestin et.al., "Cross wavelet analysis: Significance testing and pitfalls."

[7]Moreover, it is advised not to use global wavelet spectrum to determine the relative magnitude of the peaks if there exists sharp peaks in the power spectrum.
(*http : //paos.colorado.edu/research/wavelets/faq.html#orthogonal*)

absolute value of the complex coefficients, as obtained using complex morlet mother wavelet, have been plotted. Interesting features of the maps are the existence of several horizontal rows of (here, orange-red) blobs which are separated by fixed time intervals. These represent cycles in the signal. The blobs indicate a high value of the coefficient on a typical local scale because of the local scaling.

The plots are subdivided into four columns, where the left most part presents the wavelet power spectrum of the considered variables, which are cosmic ray flux, sunspot number and precipitation, each of which presents the annual variation of the normalized data variable. Since the time series is of limited duration certain spectral analysis errors will occur at the beginning and end of the spectrum. Thus, to distinguish the edge effects, a black contour is projected on to the wavelet power spectrum map to exhibit the cone of influence. It depicts the time duration or interval over which edge effects become important and is defined as the e-folding time for the auto-correlation of the wavelet power at each scale, where the $e-folding$ time equation depends on the mother wavelet (Torrence and Compo,1998) and the length of the time series. The region outside the black contour, in the first part of the figure, is the COI. The second column portrays the wavelet power spectrum outside the cone of influence. Global wavelet power spectrum is shown in the third column. Here, the horizontal axis denotes the power, and the vertical axis the period in years. The wavelet power over different period bands as the percentage of total wavelet power is illustrated in the last column.
Localscaling at each scale reveals the highest power at each scale, which even might be very small while considering all the values. In this method, Every single wavelet transform coefficient is normalized by the highest valued coefficient at that scale.

5.4 Exploring Periods in Different Period Bands

The following images illustrate the existence of power in each period band. The data series has been divided into six linear period bands, comprising 5 years each. The distribution of time periods are as follows: (1) 1 to 5 years (2) 6-10 years (3) 11 to 15 years (4) 16 to 20 years (5) 21 to 25 and (6) 26 to 30 or 28 or 27 years depending upon the data available for the station considered.

5.4.1 Power in a period band for an undamped pendulum

As an example of the method applied, we have considered a known harmonic oscillator, like an undamped pendulum, having a period of 10 cycles/time and unit amplitude. As there are 100 data points and each band corresponds to 10 points, thus the total power is distributed in 10 discrete bands ranging from 1 to 10, 11 to 20, 21 to 30, 31 to 40, 41 to 50, 51 to 60, 61 to 70, 71 to 80, 81 to 90 and 91 to 100 cycles/time. From figure(5.1) it is clear that the maximum power in the signal having a period of 10 cycles/time occurs in the first band which corresponds to a period range between 1 to 10 cycles/time. The same procedure is applied to other signals too to detect the power in different bands. The power bands of precipitation and cosmic ray flux are compared at each of the previously mentioned neutron monitor stations. The occurrence of higher power in common bands would mean possible connection between these variables. For instance, occurrence of precipitation and cosmic ray flux after every 10 years at a station with a lead or lag. This may indicate the possibility that one parameter influences the other.

The idea behind finding the period bands is that the common period bands between precipitation and cosmic ray flux at a station would provide some evidence of a relation of one parameter with the other, for instance, the dependence of precipitation on cosmic ray flux. Hence, we will be able to conclude that cosmic ray flux, along with the other climatic variables, influence the precipitation on earth at the considered location. In the following sections, we consider each parameter at every considered station.

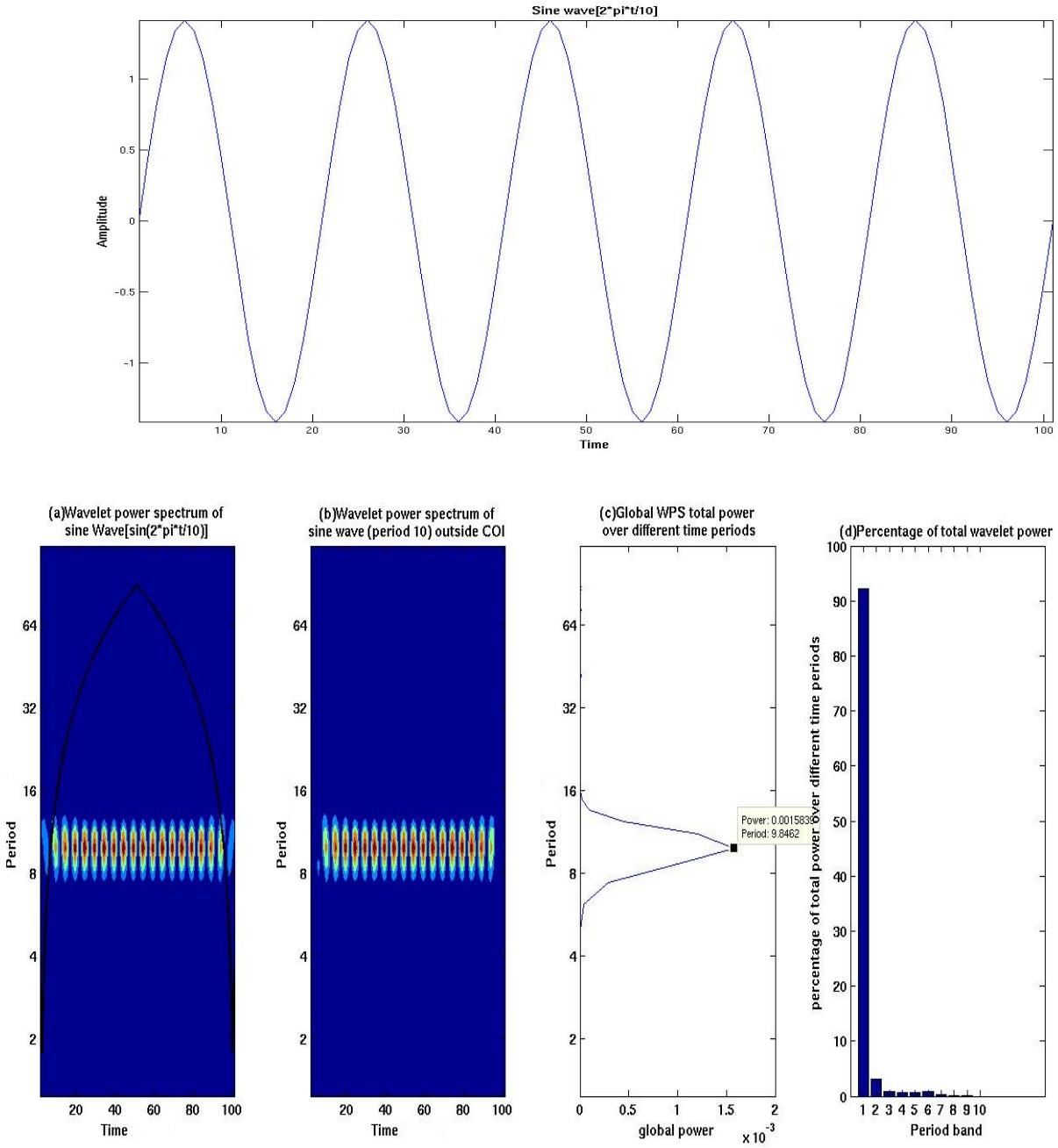

Figure 5.1: Wavelet Power over different period bands as percentage of total wavelet power of the known *sine* wave

5.4.2 Wavelet spectra of cosmic ray flux and precipitation at Thule

The global wavelet power spectra in figure(5.3(c)) and figure(5.2(c)) show a dominant cycle of 9.8 years in the case of precipitation and cosmic ray intensity at

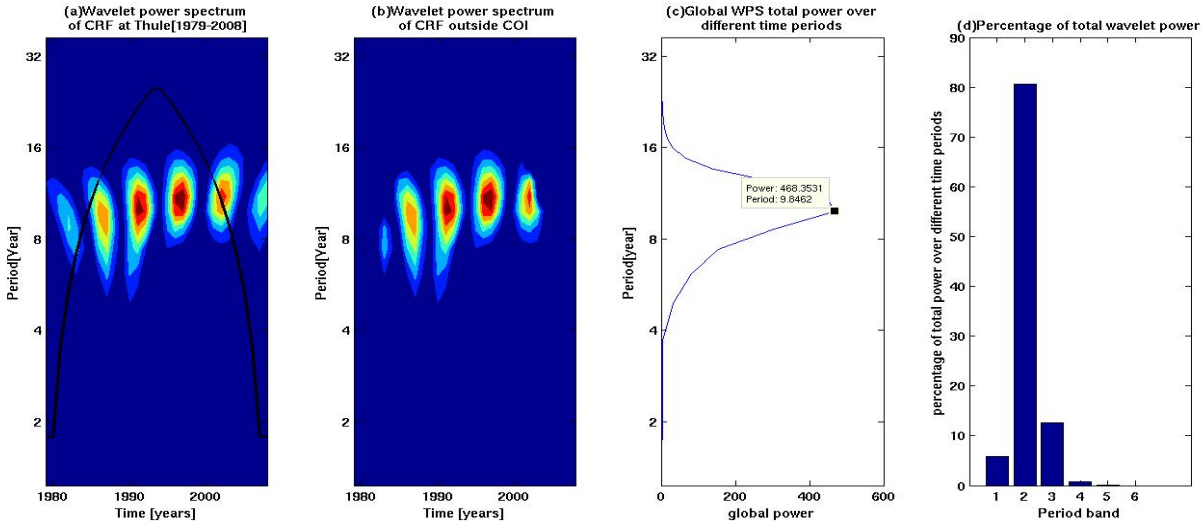

Figure 5.2: Wavelet Power of cosmic ray flux at Thule, over different period bands as percentage of total wavelet power.The power is clearly high in the band 2 of the wavelet power spectrum, which range from 6 to 10 years period.

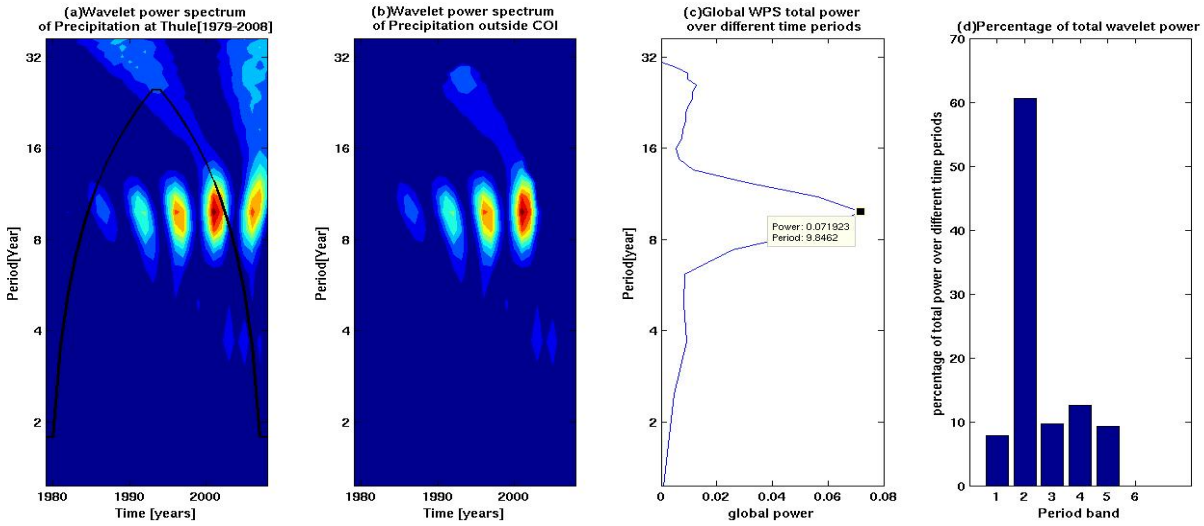

Figure 5.3: Wavelet spectra of Precipitation at Thule, over different period bands as percentage of total wavelet power

Thule. Thus, we can conclude that both the phenomena occur after an interval of 9.8 years with CRF leading precipitation in time. Accordingly, power is high in the band 2, figure(5.2(d)), of the wavelet power spectrum, which ranges from a 6

to 10 year period. The power in this band contributes to 80% and 62% of the total power of cosmic ray flux and precipitation respectively.

Conclusion

As can be seen in the in figure(5.2(a)) and (5.3(a)), the maximum power lies in the 9.8 or 10 year cycle. This common period and power in the common band between the two variables suggests the conclusion that there is a dependency of precipitation on cosmic ray flux at Thule. A peak in the global power in figure 5.3(c) and figure 5.2(c) at 10 years presents the common cycle. This common periodicity points towards a relation between cosmic ray flux and precipitation at Thule. Thus one may influence the other with a lead of days or months or even years. The data considered here is from January 1997 to December 2008. This time ranged constitutes complete 21st and 22nd solar cycle, which are small cycles of approximately 10 years on average[8]. Thus, the period of 10 years found in the CRF time series can be accounted by the solar cycle during the period.

5.4.3 Wavelet spectra of cosmic ray flux and precipitation at Climax

Figure(5.4) exhibits the wavelet cone of influence (COI) wavelet power spectrum outside the COI, global wavelet power spectrum and the percentage of the total wavelet power over different bands. Looking at the fourth, vertical, subplot in the figure, we may notice that the maximum power lies in the 6 to 10 year period band.

The highest power in the wavelet power spectrum of precipitation at Climax, figure(5.5), lies in band 2 that corresponds to a time interval from 6 to 10 years and contributes to 74% and 47% of the total power of cosmic ray flux(CRF) and precipitation respectively. The second highest power is observed in band 3 which constitutes 15% in the case of CRF and 37% in the case of precipitation at the station. As can be seen from the global wavelet power spectrum, the dominant cycle is of 12.3 years.

[8]S.K. Pandey, Rahul srivastave, LK borkar, AK tripathi, Aka tripathi and SC dubey, , 10June 2010, Research Communications, Current Science, "Study of sunspots and sunspot cysles 1-24" Vol.98, No.11, 10June 2010

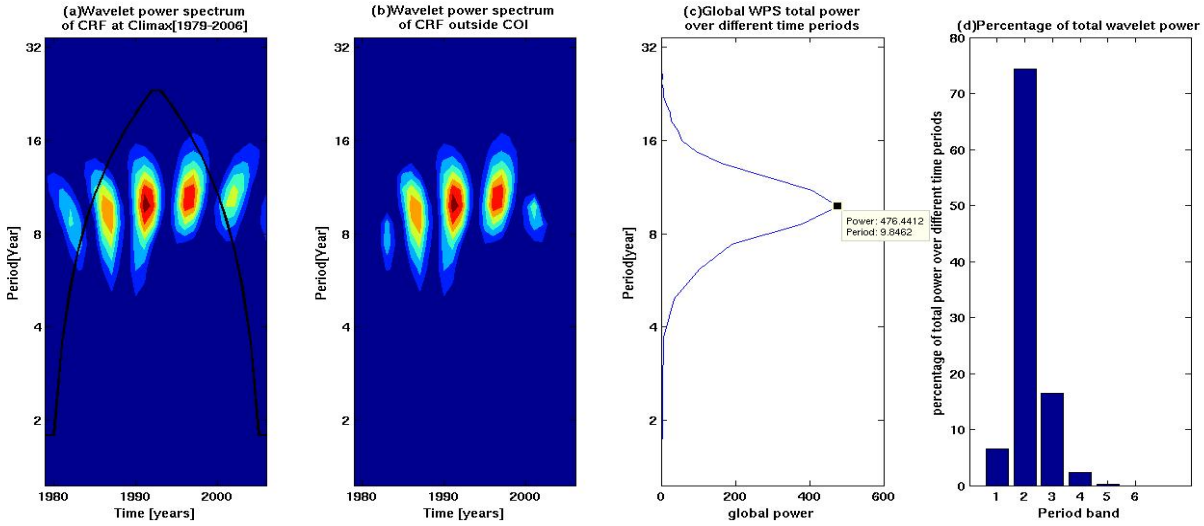

Figure 5.4: Wavelet Power of cosmic ray flux at Climax, over different period bands as percentage of total wavelet power

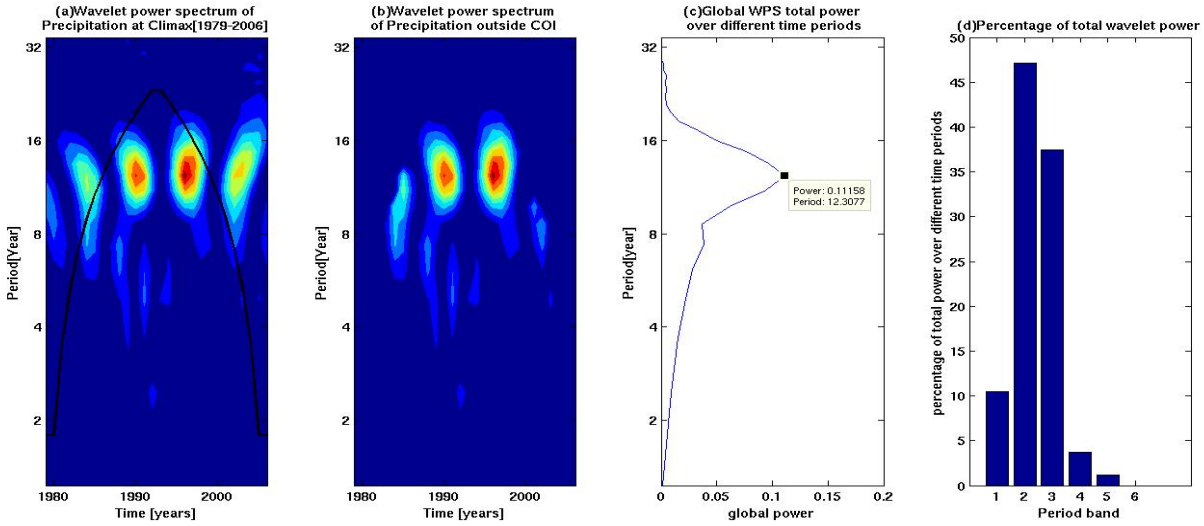

Figure 5.5: (a)Wavelet spectra of Precipitation at Climax neutron monitor station,(c)The global Wavelet power spectra of Precipitation at Climax and (d)different period bands as percentage of total wavelet power

Conclusion

As can be inferred from the two figures above, the cosmic ray flux along with the other parameters contribute to the precipitation at Climax neutron monitor

station.

5.4.4 Wavelet spectra of cosmic ray flux and precipitation at Huancayo

The percentage of power is noticeably higher in bands 2 and 3 for cosmic ray flux and in bands 1 and 2 for precipitation. Thus the cosmic ray flux at Huancayo reveals a periodicity the period band between 6 to 10 years along with the period band between 11 to 15 years. At Huancayo, the power contributed by the precipitation parameter is higher in the period bands of 1 to 5 years and 6 to 10 years.

5.4.5 Wavelet spectra of cosmic ray flux and precipitation at Namibia

The 6 to 10 year band shows higher percentage of power in cosmic ray flux signal at Namibia and lies in the band 2. The power in this band corresponds to 83% of the total power in the wavelet power spectrum. However, bands 1, 2 and 3, shows higher fraction of power in precipitation signal at Namibia. The power distribution ,figures (5.8)(d)) and (5.9)(d), are dissimilar. Thus we may infer that parameters other than cosmic ray flux also contribute to precipitation in equatorial regions. The 26 to 30 year period band contains 24% of total power about 20% and the band 5 , corresponding to 21 to 25 years.

5.4.6 Wavelet spectra of cosmic ray flux and precipitation at Potchefstroom

Like all other stations, the CRF at Potchefstroom too shows a cycle of 9.8 years as the major cycle and hence the highest power is in band 2. At Potchefstroom, CRF signal contributes to 84% of the total power in the signal. Precipitation at Potchefstroom shows periods 2 and 1 as the higher power bands. Moreover, both the parameters shows a common period of 9.8 years. Thus cosmic ray flux seems to affect precipitation at the station.

The band 2 makes the greatest contribution of 74% to the total wavelet power.

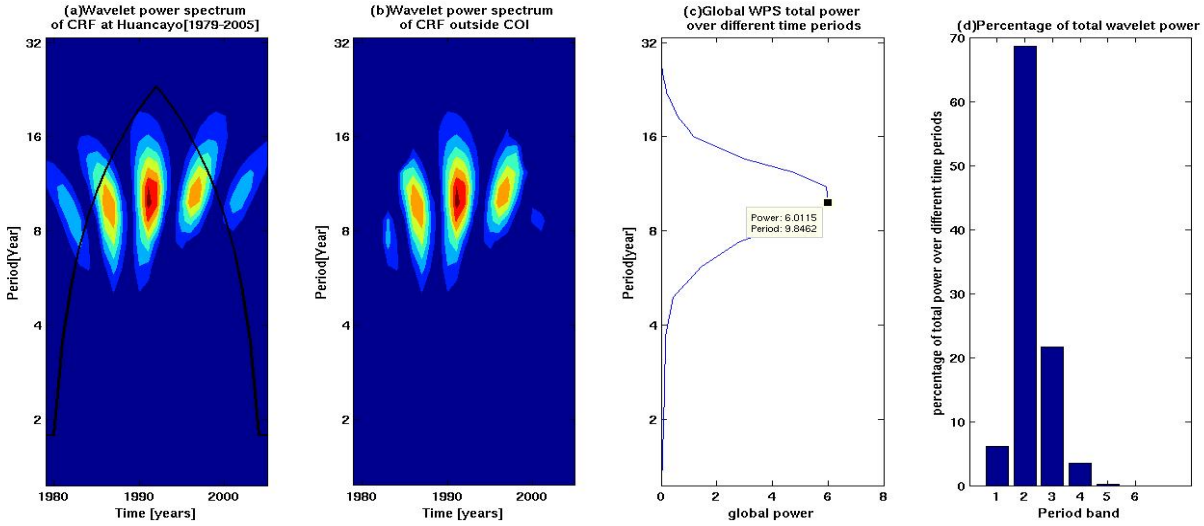

Figure 5.6: Wavelet Power of cosmic ray flux at Huancayo, over different period bands as percentage of total wavelet power

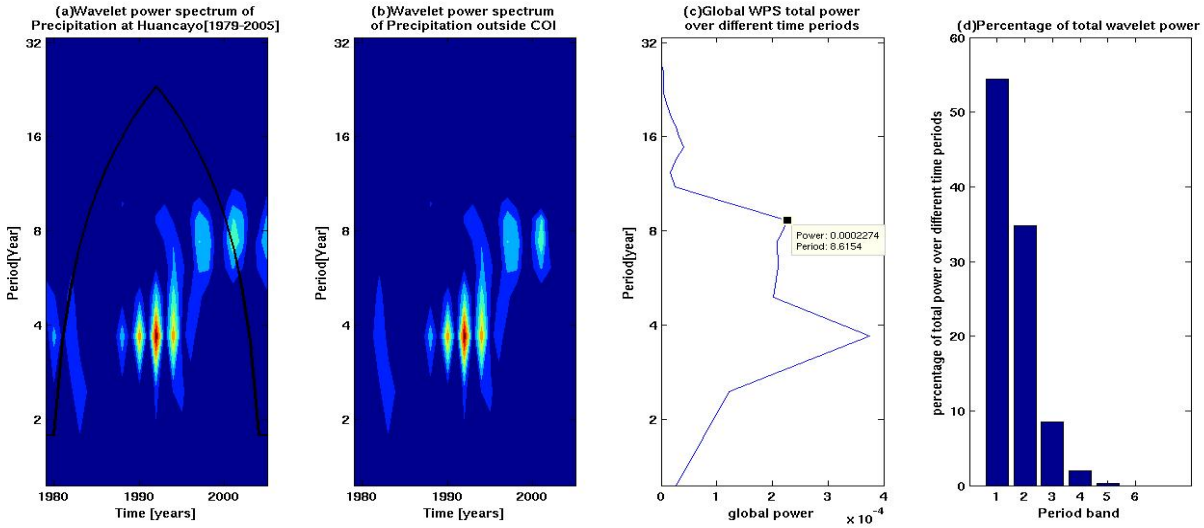

Figure 5.7: Wavelet spectra of Precipitation at Huancayo neutron monitor station, over different period bands as percentage of total wavelet power

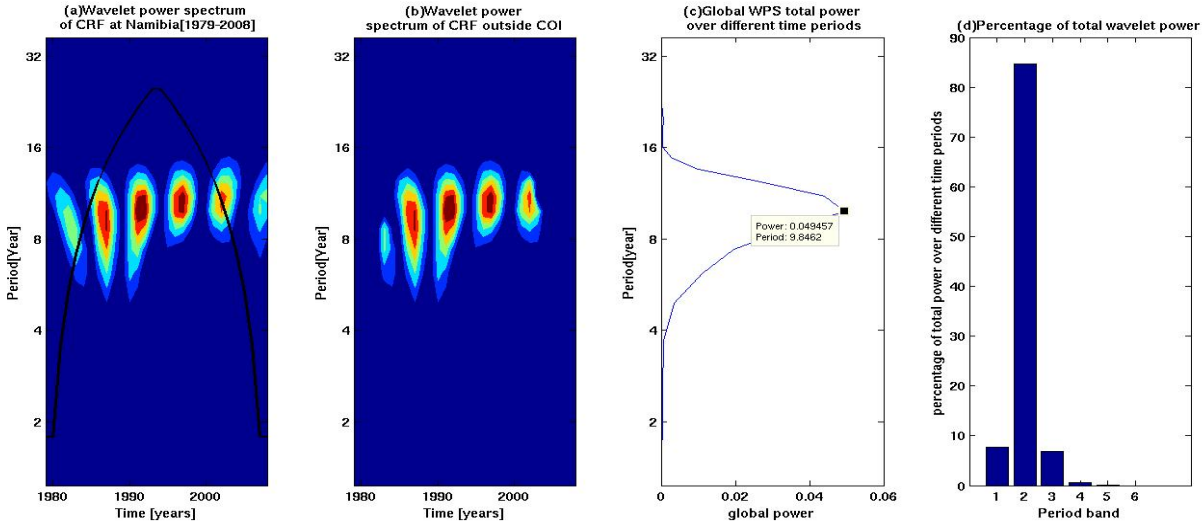

Figure 5.8: Wavelet Power of cosmic ray flux at Namibia, over different period bands as percentage of total wavelet power

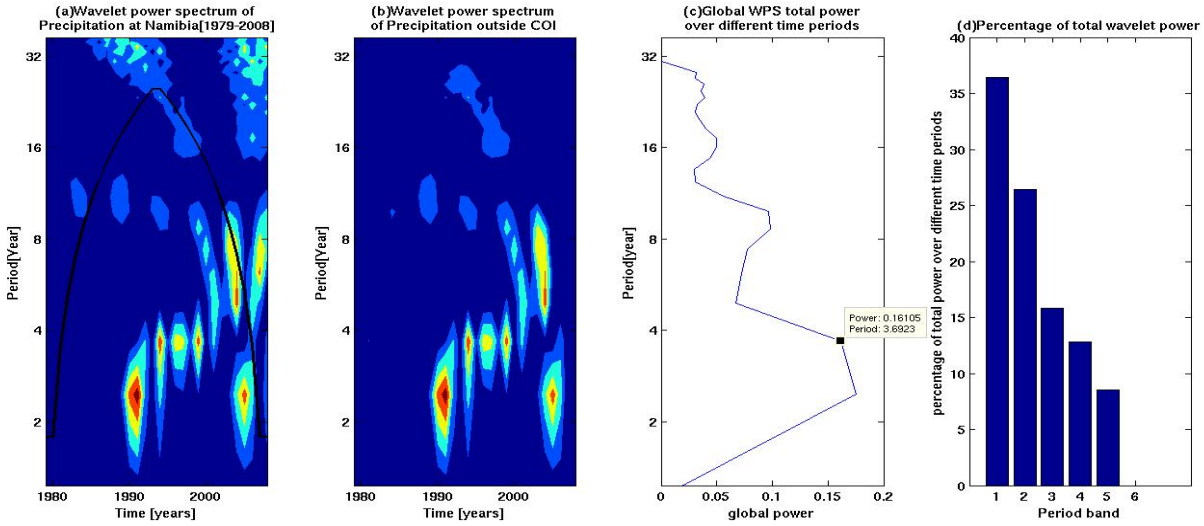

Figure 5.9: Wavelet spectra of Precipitation at Namibia neutron monitor station, over different period bands as percentage of total wavelet power

5.4.7 Wavelet spectra of Cosmic ray flux and Precipitation at Hermanus

From figure(5.12) we notice that, of the total power in the CRF wavelet power spectrum of cosmic rays at Hermanus, 82% lies in band 2, (6 to 10 years). Similarly,

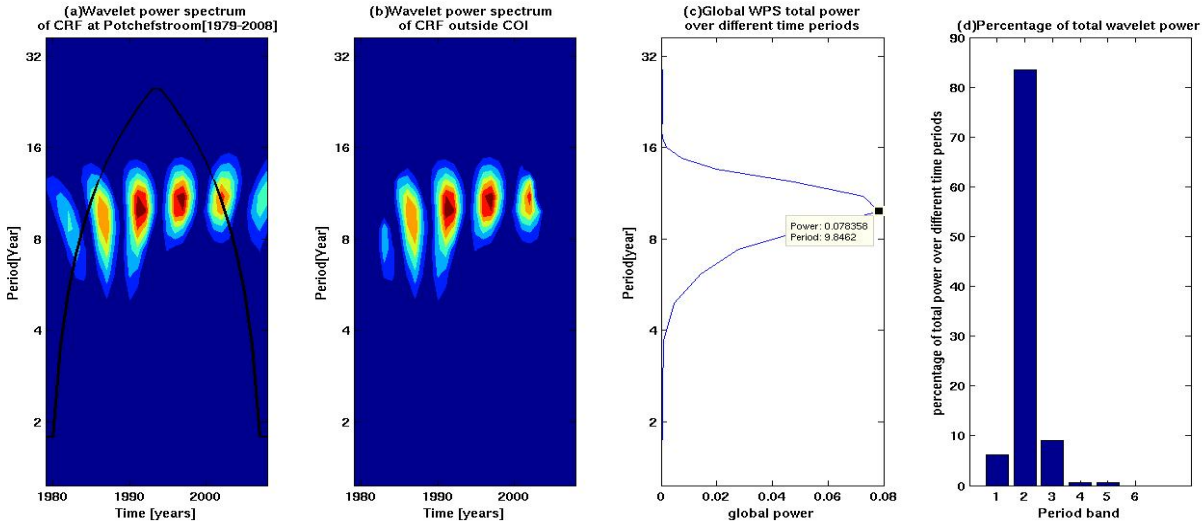

Figure 5.10: Wavelet Power of cosmic ray flux at Potchefstroom, over different period bands as percentage of total wavelet power

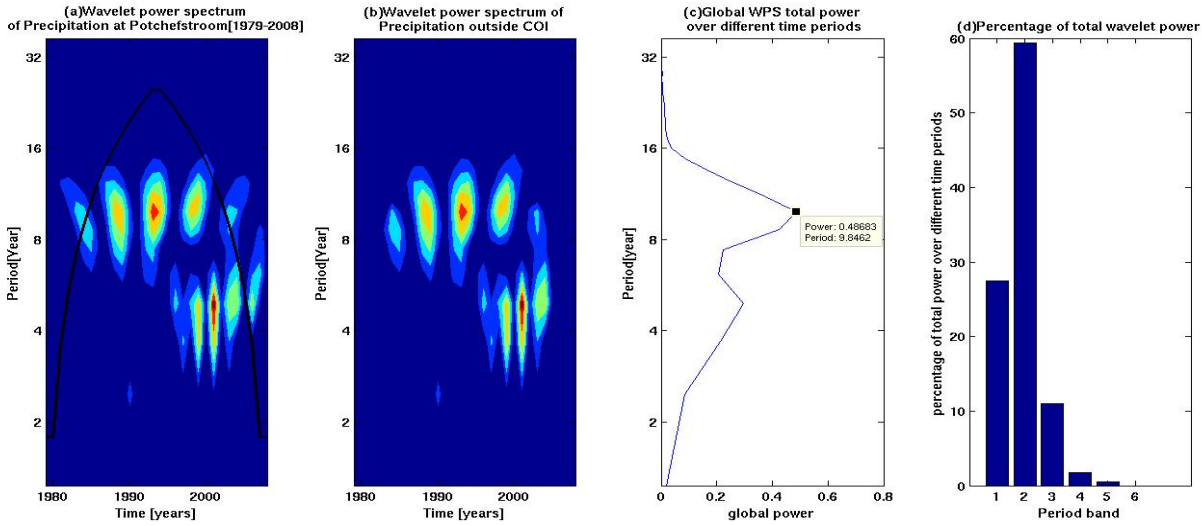

Figure 5.11: Wavelet spectra of Precipitation at Potchefstroom neutron monitor station, over different period bands as percentage of total wavelet power

band 2 also makes the highest contribution to the total power in precipitation at Hermanus. Moreover, the power distribution is similar for both variables at the station. This implies that the CRF at the station may influence the precipitation

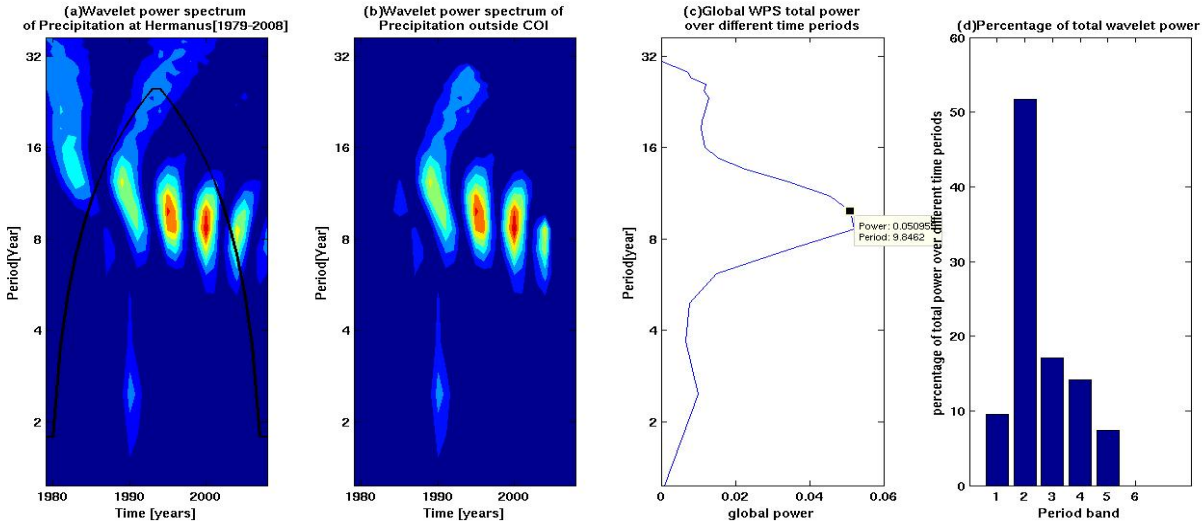

Figure 5.12: Wavelet Power of cosmic ray flux at Hermanus over different period bands as percentage of total wavelet power

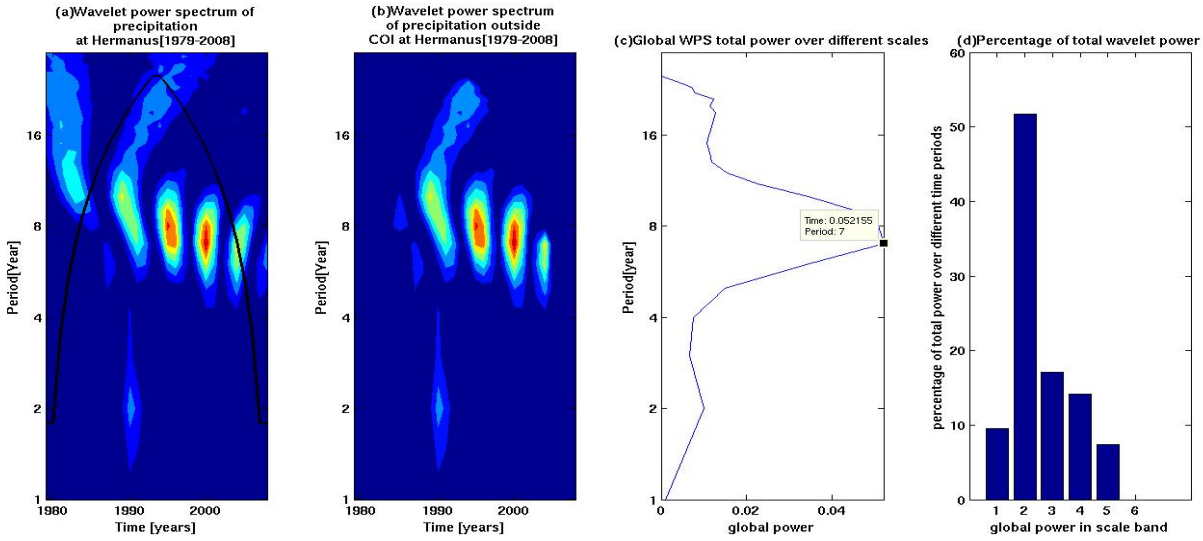

Figure 5.13: Wavelet Power of precipitation at Hermanus neutron monitor station over different period bands as percentage of total wavelet power

at Hermanus during the of 30 year, for which data sets are available.

Bands 2 and 5, (6 to 10 and 21 to 25 years respectively), contribute to 29 and 18 % of the total wavelet power, as illustrated in figure(5.13).

5.4.8 Power in a period band for solar activity

The dominant cycles of 9.8 and 11 years are clearly visible in the global wavelet power spectrum of the sunspot number, figure(5.14(b)), the quasi-stationary solar cycle, in figure(5.14(a)), and the highest power in period band 2 can be noticed in figure(5.14(d)). Thus during the considered interval of time, 1979 to 2008, a 9.8 or 10 years period is noticed in the wavelet power spectrum of the sunspot number and this corroborates with the periodicity we obtained in chapter(4). Along with this 10year oscillation, a period of 11 years is also visible in the figure(5.14). This cycle was however, not obtained in the power spectrum of sunspot number in chapter(4), using welch power spectrum method.

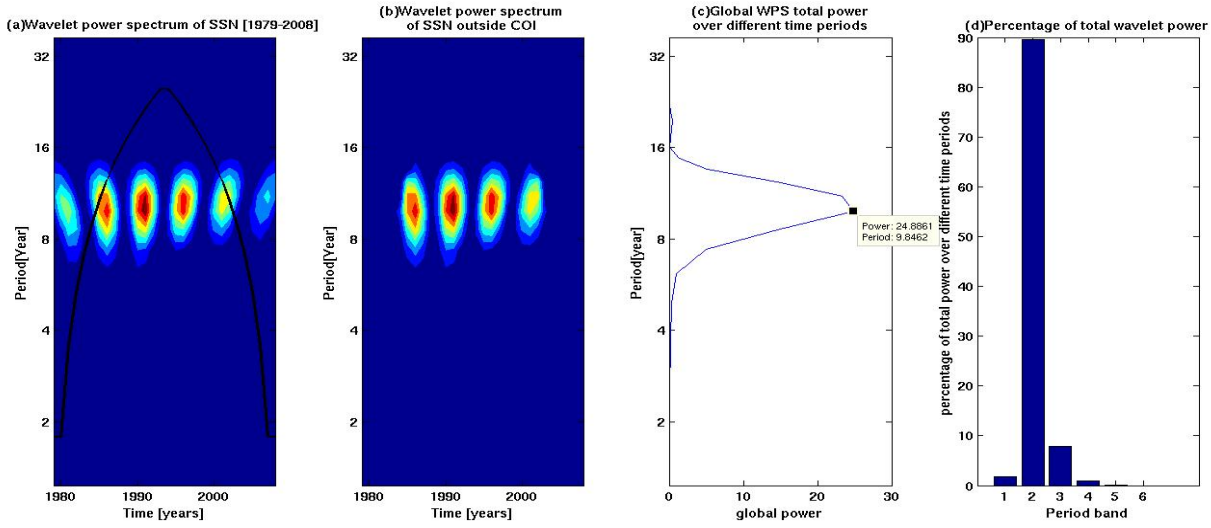

Figure 5.14: (a)Wavelet spectra of sunspot number signifying a quasi-stationary sunspot cycle from 1979 to 2008, (b)The global wavelet power spectrum of the sunspot number and (c) Wavelet power in different power bands

5.4.9 Percentage of total wavelet power for cosmic ray flux and precipitation at six different latitudes and longitudes(without local scaling)

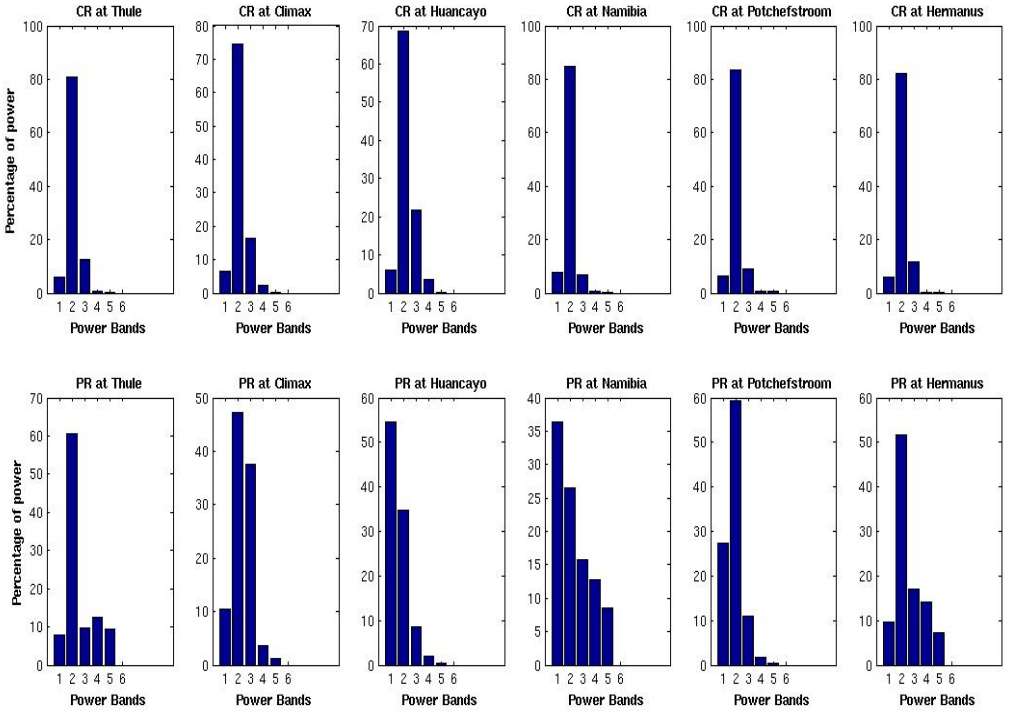

Figure 5.15: Percentage of total wavelet power for cosmic ray flux(first row) and precipitation (second row) at all the previously mentioned neutron monitor stations, over different period bands

The figure (5.15) represents the percentage of total wavelet power for cosmic ray flux and precipitation at the six selected neutron monitor stations. From this figure, it can be inferred that cosmic ray flux and precipitation share band 2 as the one with the highest power at the stations above 26° N and beyond 39° S latitudes. Further, the table below presents the band with greatest power, averaged over different period bands in the wavelet power spectrum of cosmic ray flux and precipitation at all the neutron monitor stations considered. The annual sunspot and cosmic ray flux data have been considered for a period of thirty years, from 1979 to 2008. The

thirty data points are normalized before computing the correlation coefficients.

Station	Latitude	Major Bands[Years]		Dominant cycles[Years]	
		CRF	Precipitation	CRF	Precipitation
Thule	76.5 N	6-10	6-10	9.8	9.8
Climax	37.37 N	6-10	6-10	9.8	12.3
Huancayo	12.03 S	6-10	1-5	9.8	3.6
Namibia	19.12 S	6-10	1-5	9.8	2.4
Potchefstroom	26.41S	6-10	6-10	9.8	9.8
Hermanus	34.25 S	6-10	6-10	9.8	7

Table 5.1: Table illustrates the wavelet power bands corresponding to highest power and the dominant cycles in cosmic ray flux and precipitation signal at the six considered stations. The first two columns show the considered stations and the corresponding latitude, third and fourth columns present the highest power band in CRF and precipitation respectively; fifth and sixth columns portrays the dominant cycles in each of the parameters at the station

5.5 Conclusion:

1. As the highest band power in the case of cosmic ray flux at all the considered neutron monitor stations is no.2, we can infer that the cosmic ray flux does not vary much over latitudes.

2. We notice a symmetry in the distribution of power bands across the globe. Precipitation signal at the stations beyond 26° south and above 39° north contributes to the power band 2 as the common band denoting the highest power in the case of cosmic ray flux and precipitation as well. Thus, the cosmic ray flux over the mentioned regions could appreciably influences the precipitation at those locations.

3. The sunspot cycle length oscillates between 9 to 14 years[9]. The wavelet power spectrum of the sunspot number after global scaling shows the presence of a 9.85 or 10 year cycle as the dominant one during the time period from 1979 to 2008.

[9] $http://en.wikipedia.org/wiki/Solar_cycle$

CHAPTER 6

POINT PROCESS ANALYSIS OF WTC MAXIMA USING WAVELET MAPS

6.1 Wavelet Map and WTC Maxima Phase Difference

In the present chapter we pose a very useful method for analysing the possible relations between cosmic processes and monsoon rainfall. This work is motivated by the wavelet maps of Kailas and Narsimha,2000 and Narsimha and Kailas, 2001, who applied the method to study homogeneous Indian monsoon rainfall for a period 1870 to 1990. Wavelet maps represent the absolute value of the wavelet transform coefficients (WTC) for the considered time series. Here, the objective of our study is to check for the presence of structures and patterns in the WTC maps. Similarities in the patterns of two time series can suggest possible connections between the two time series considered. For our analysis, we take WTC maxima in the wavelet maps of CRF and precipitation at Thule around a scale of 10 years. The reason behind considering a band around 10 years is because of the presence of a 10 year period in the CRF and precipitation time series at Thule during the 22nd and 23rd solar cycle. Then we attempt to find the time lag if any between the WTC maxima of the considered signals.
First, we find WTC maxima in annual CRF and precipitation data at Thule.

6.1.1 Wavelet Map of Annual CRF and Precipitation at Thule

The wavelet maps of CRF and precipitation are presented in figure(6.1 and 6.2) respectively. In each of the wavelet maps, we can notice a similar pattern of blobs. Within each blob, we locate the maximum WTC and we get figure(6.3). Here, the red dots indicate the WTC maxima of CRF time series and blue the precipitation; both around a wavelet scale of 10 years.

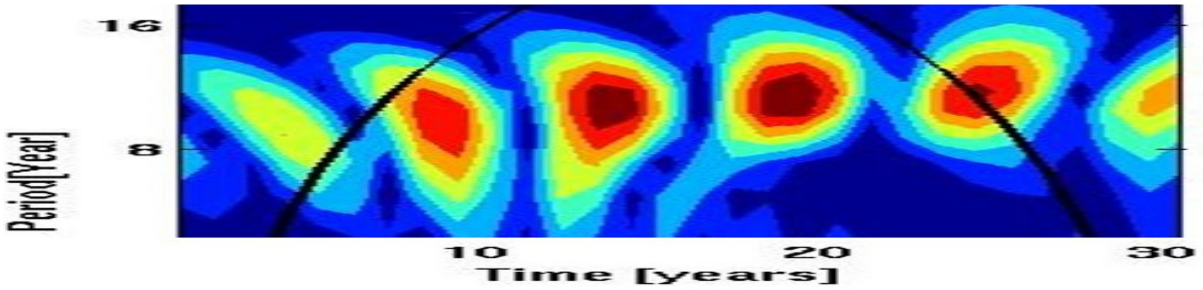

Figure 6.1: Wavelet map of annual CRF at Thule[1979 - 2008]

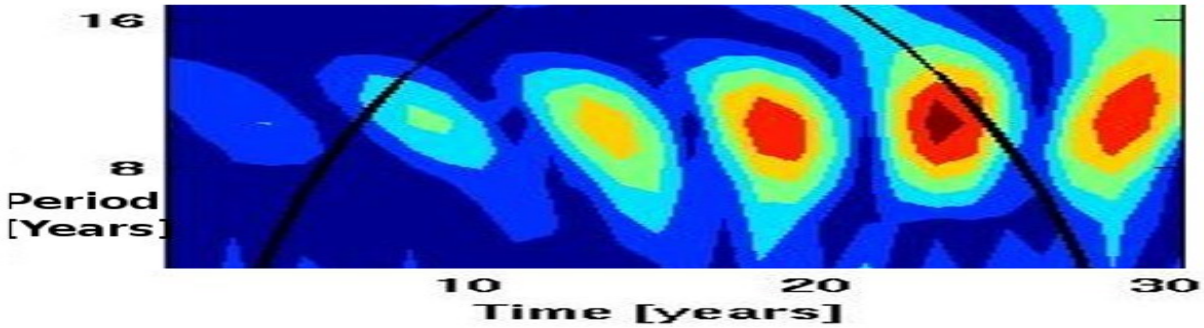

Figure 6.2: Wavelet map of annual precipitation at Thule[1979 - 2008]

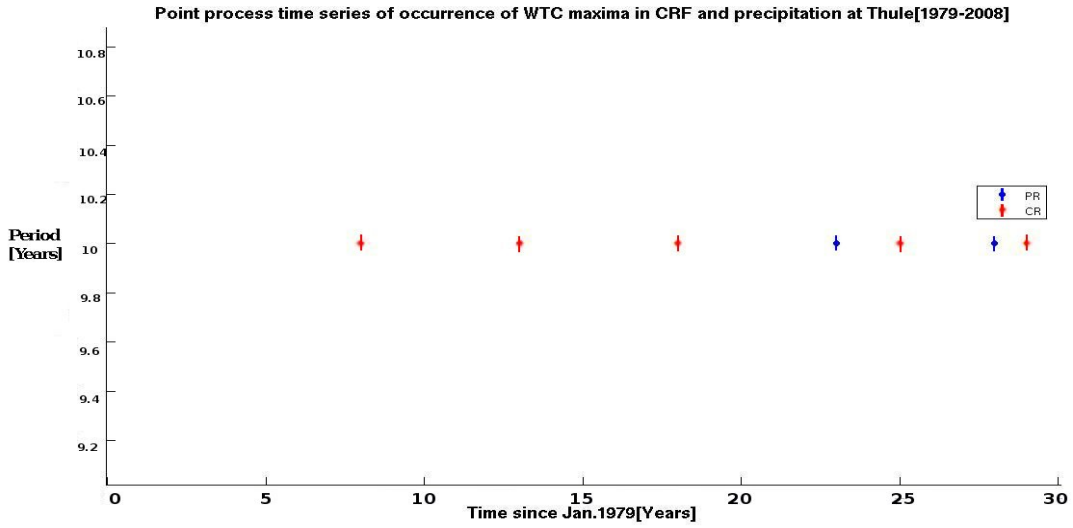

Figure 6.3: WTC maxima in annual CRF and precipitation at Thule[1979 - 2008]

As we can see in figure(6.3), the WTC maxima of annual CRF and precipitation first overlap over the period from 1987 to 1997, and then CRF appears to lead.

The time difference after 2004 lies in the cone of influence and is not significant. As we do not have enough points showing a time difference, we cannot infer the presence or absence of any time difference with confidence using annual CRF and precipitation time series. Thus, we need more data points or a longer data set to determine any significant phase difference. Moreover, as we could not find any significant time difference between the two signals using annual data, perhaps the time difference between the two time series is less than an year. Thus, we carry out similar analysis with the monthly data set.

6.1.2 Wavelet Map of Monthly CRF and Precipitation at Thule

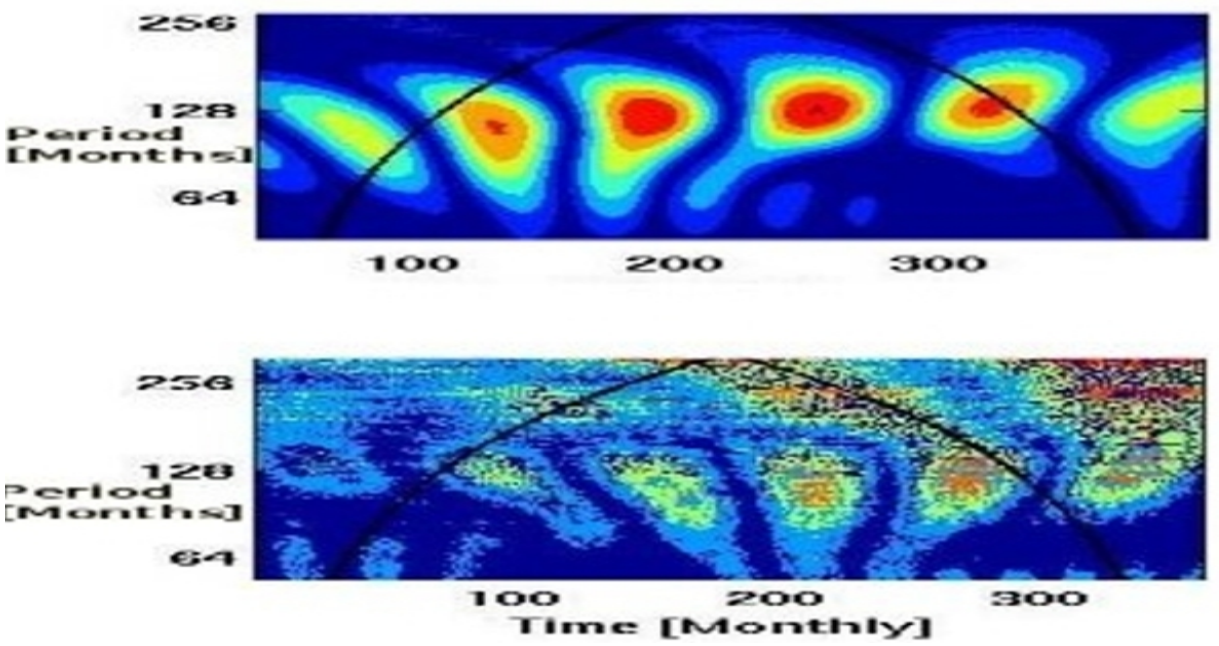

Figure 6.4: Wavelet map of monthly CRF and precipitation at Thule around a period of 10.66 years or 128 months

Like for the annual data, we take the WTC maxima around a period of 10 years. The wavelet maps of monthly CRF and precipitation at Thule is shown in figure(6.4). The phase point wavelet map for monthly data can be seen in figure(6.5). From the figure(6.5), the CRF leads the precipitation at Thule. The time differences are 1,2 and 9 months. However, time difference between the CRF

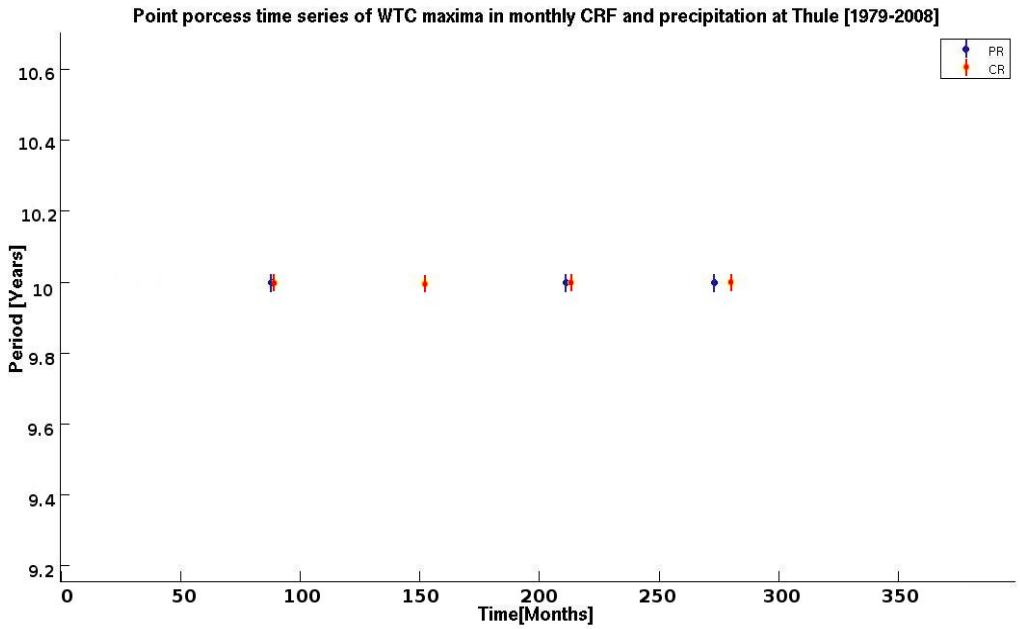

Figure 6.5: WTC maxima in monthly CRF and precipitation at Thule[1979 - 2008]

and precipitation is not consistent. Thus we can not come to any definitive conclusion about the time difference with a acceptable confidence.

To summarize, the precipitation and CRF wavelet maps exhibit striking similarity in pattern of horizontal row of blobs around 10 years scale. Monthly

CHAPTER 7

CONCLUSIONS

7.1 Conclusions

This thesis presents an analysis of the possible connections between the cosmic ray flux(CRF) and precipitation over a geographically diverse latitude range. The precipitation data set has been taken from Global Precipitation Climatology Project (GPCP), which used both gauge measurements and satellite estimates of precipitation, and is considered reliable. The cosmic ray flux has been acquired from the NOAA National Geophysical Data Center. The following are the major conclusions from the thesis:

1. **Results from time domain analysis**

Station	Latitude	Correlation Coefficient
Thule	76.5 N	-0.8267
Climax	37.37 N	-0.8076
Huancayo	12.03 S	-0.7736
Namibia	19.12 S	-0.8118
Potchefstroom	26.41S	-0.8219
Hermanus	34.25 S	-0.8361

Table 7.1: Table illustrating the correlation coefficient, above 99.9% significance level, between the sun spot number and the cosmic ray data at six stations

* Time domain analysis confirms that the cosmic ray flux is anti-correlated with solar activity. The anti-correlation can be explained by the effect of sun's magnetic field which deflects the CRF while entering the heliosphere. The correlation between the CRF and SSN vary between -0.77 to -0.83 and increases only slightly with decreasing latitude, but remains almost constant. Thus, CRF and solar intensity vary weakly with latitude.

Station	Correlation Coefficient	P-value	Duration
Thule	0.0275	0.7238	1994 to 2007
Climax	0.0135	0.8495	1994 to 2007
Huancayo	0.0033	0.9072	1994 to 2007
Namibia	-0.0376	0.6287	1994 to 2007
Potchefstroom	0.0193	0.8073	1994 to 2007
Hermanus	-0.0322	0.6785	1994 to 2007

Table 7.2: Correlation Coefficient, and corresponding p-values and (indicating varying significance level)m, between the low-cloud cover and the Cosmic Ray flux data at six stations during the time interval, Jan1994 to Dec2007

* CRF does not seem to significantly influence low cloud cover at any of the six stations, which can be due to the short duration of the data sets available and possible calibration problems with the cloud cover data. Thus, we can not claim presence or absence of any relation between the two variables.

Station	Correlation Coefficient	P-value	Duration	Latitude
Thule	0.4633	0.0099	1979 to 2008	76.5 N
Climax	0.2583	0.1844	1979 to 2006	39.37 N
Huancayo	-0.0772	0.7020	1979 to 2006	12.03 S
Namibia	0.1558	0.4110	1979 to 2008	19.12 S
Potchefstroom	0.1071	0.5733	1979 to 2008	26.41 S
Hermanus	0.1594	0.4002	1979 to 2008	34.25 S

Table 7.3: Correlation coefficient and the corresponding p-value between precipitation and cosmic ray intensity data at six stations are furnished in the table above. The correlation coefficient is significantly high at Thule neutron monitor station

* CRF significantly correlates with the precipitation at only one of the six considered stations, Thule, which is located about 14,° south of the north pole. Thus, precipitation at higher latitudes seems to be affected by the CRF. Perhaps due to the geomagnetic shielding which deflects the CRF towards the poles. Thus a strong amount CRF collects at polar regions to influence the atmosphere by ionizing it. These ions would then lead to formation of ultra-fine aerosols that can act as CCN, and can effectively influence the global electric circuit which helps in enhancing ice nucleation in clouds. These

clouds then precipitate under proper conditions of pressure and temperature. The precipitation at poles is mainly in the form of snow. And as the CRF helps in ice nucleation, the precipitation at higher latitudes may be explained by the effect of CRF.

Station	Correlation Coefficient	P-value
Thule	-0.5158	0.0009
Climax	-0.3846	0.0433
Huancayo	0.0580	0.7739
Namibia	-0.0800	0.6744
Potchefstroom	-0.0162	0.9324
Hermanus	-0.1864	0.3239

Table 7.4: Correlation coefficient and corresponding p-values between precipitation and the sun spot data at six stations

* Precipitation is anti-correlated with the SSN at five out of the six stations. And significantly anti-correlated at Thule. Only, at Huancayo, which lies in the tropics, is the precipitation weakly positively correlated with the SSN, but, the correlation is very small.

2. **Results from power spectral analysis**

Station	Cycles in cosmic ray flux	Cycles in precipitation
Thule	10(>99%),5(>95%)	10(>99%),3.3,2.7(>95%)
Climax	9.33(>99%)	15,6,2(> 95%)
Huancayo	9(>99%)	4.3(> 99%),15,2.5,3(> 95%)
Namibia	10(>99%)	3(> 99%),10(>95%)
Potchefstroom	10(>99%),2.3(>95%)	10(> 99%) 5,2.5,2(> 95%)
Hermanus	10(>99%),2.3(> 95%)	3(> 99%) 10(> 95%)

Table 7.5: List of cycles in cosmic ray flux and precipitation at six stations using Auto power spectrum [Years]

* A significant cycle of 10 years in the case of both precipitation and CRF is noticed at Thule, Hermanus and Potchefstroom neutron monitor stations. As the stations share the common cycle between the CRF and precipitation, we may infer that CRF may influence the precipitation at the stations. Which again might be explained due to geomagnetic shielding.

3. **Results using wavelet power spectrum analysis:**

Station	Latitude	Major Bands[Years]		Dominant cycles[Years]	
		CRF	Precipitation	CRF	Precipitation
Thule	76.5 N	6-10	6-10	9.8	9.8
Climax	37.37 N	6-10	6-10	9.8	12.3
Huancayo	12.03 S	6-10	1-5	9.8	3.6
Namibia	19.12 S	6-10	1-5	9.8	2.4
Potchefstroom	26.41S	6-10	6-10	9.8	9.8
Hermanus	34.25 S	6-10	6-10	9.8	7

Table 7.6: Table illustrates the wavelet period bands corresponding to highest power and the dominant cycles in cosmic ray flux and precipitation signals at the six considered stations. The first two columns show the considered stations and the corresponding latitude, the third and fourth columns present the highest power band in CRF and precipitation respectively. The fifth and sixth columns list the dominant cycles in each of the parameters at the station

* It can be observed from table(7.6) that at all the six considered stations, a dominant cycle of 9.8 years is present. Thus, we may confirm that the CRF

does not vary much across the latitudes. A global oscillation of 9.8 years is present in the CRF throughout the 30 years period, from 1979 to 2008. The global cycle of 9.8 years can be observed in the precipitation at Thule and Potchefstroom neutron monitor stations. This may account for the relation of CRF with the precipitation at higher latitudes.

* CRF and precipitation time series are quasi-stationary in nature.

4. **Result from wavelet map and point process method:**

Significant Period band	Time difference
118	2 months

Table 7.7: Table illustrating the time difference, using point phase method and wavelet maps, between the cosmic ray flux and precipitation at Thule

* The CRF significantly influences the precipitation at Thule. The CRF leads the precipitation by a period of approximately 2 months.

* To sum up all, the data analysis methods applied so far point toward possible influence of CRF on precipitation at high latitudes. Apart from correlation and power spectrum analysis, wavelet transforms especially helped in detecting a common cycle of 9.8 years in both CRF and precipitation time series.The method also helped in detecting the non-linearity and non-stationary character in the time series considered. Thus, the wavelet transform pose as a very powerful tool to analyse non-stationary and non-linear time series.

* After analysing the annual data, we could not find significant consistent phase difference between the CRF and precipitation. Thus, if the phase difference exists, it is perhaps less than an year.

* A physical process to explain the observation can be put together as follows. Charged cosmic particles collide with the earth's atmosphere and ionize it. Water molecules are polar in nature and hence have greater tendency to get attracted to the charged particles. Now, as the water droplets come close to the charged particles in the atmosphere, they get attracted towards these ions

and the accumulation grows with time. And when the accumulation reaches a critical level, it precipitates under the right conditions.

* From the wavelet maps the time difference between the CRF and precipitation are 1,2 and 9 months, but is not consistent. Thus we cannot come to any definitive conclusion about the time difference.As, the data considered for the analysis spans only a duration of 30 years, or 3 solar cycles, we cannot make a confident statement about the time lag. To confirm the mentioned relation with confidence, data sets of longer duration are advised.

* *Mechanism to explain the variation of correlation between CRF and Precipitation with latitudes:* We have observed significant influence of CRF on precipitation at the Thule neutron monitor station. However, the effect is negligibly small at lower latitudes. This may be explained as follows. Perhaps, at higher latitudes the number of CCN is very small. Therefore, considerable amount of CRF may cause dramatic change in CCN at those latitudes. At equatorial regions, other factors like atmospheric circulation, ocean currents, and higher solar flux may overthrow the effect of CRF.

7.2 Vistas Ahead

We believe that this thesis has throw some light on the currently ongoing research for possible connections between the GCR flux and such atmospheric parameters as precipitation. It is possible to devise mathematical and statistical tools that can detect, with considerable confidence, the influence of cosmic attributes on atmospheric parameters such as cloud cover and precipitation even with sample size of a few decades. Methods used in the thesis, for instance wavelet map, can be thought of adding considerable value to the analysis of non-stationary time series. To take the work further, statistical methods for significance testing in wavelets can be applied. Considering longer data set would provide more confidence to the results posed here.
We believe that the ideas and methods used here have wide applicability in analyzing parameters triggering considerable change in our climate.

Appendix

From the fig.(1),fig.(2), fig.(3), fig(4), fig(5), and fig.(6) we can see that the maximum value of the CRF at Thule, Climax and Huancayo during the considered time period are 4700, 4300, 1770, 3100, 100, & 100 and the overall minima are 3300, 3000, 1540, 2500, 80, & 76 respectively. Normalized data of this absolute data at the mentioned stations has been used in Chapter 2, figure(2.7). The maximum values of the CRF at the stations can help us to to estimate the threshold levels above which CRF can influence precipitation. Reader should be careful while interpreting the time series at Potchefstroom and Hermanus, as it seems that some sought of scaling is done but we are not sure about the method applied.

Station	Maximum CRF value	Minimum CRF value
Thule	4700	3300
Climax	4300	3000
Huancayo	1770	1540
Namibia	3100	2500
Potchefstroom	100	80
Hermanus	100	76

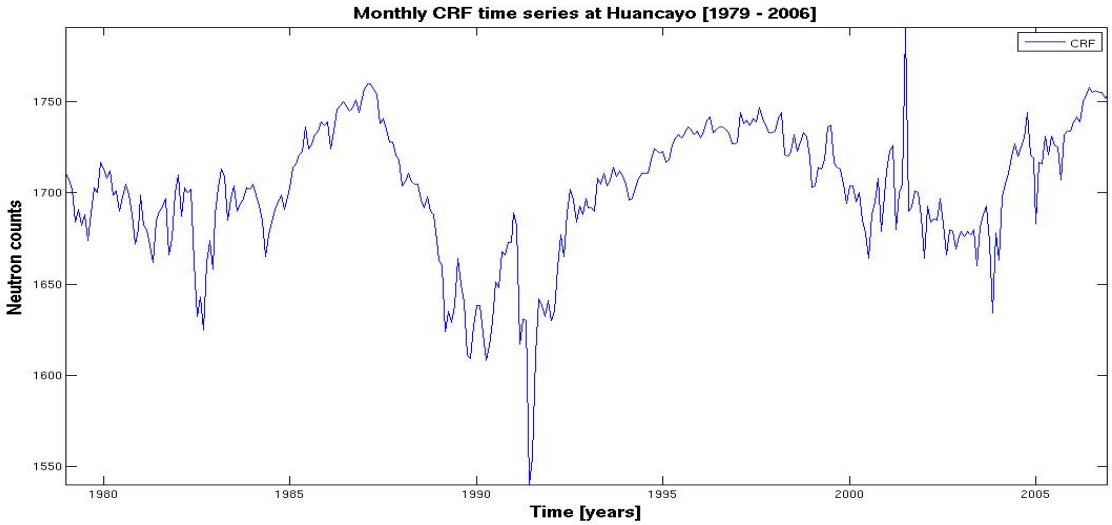

Figure 1: Time series plot of absolute (without scaling or normalization) CRF at Huancayo[1979 - 2006]

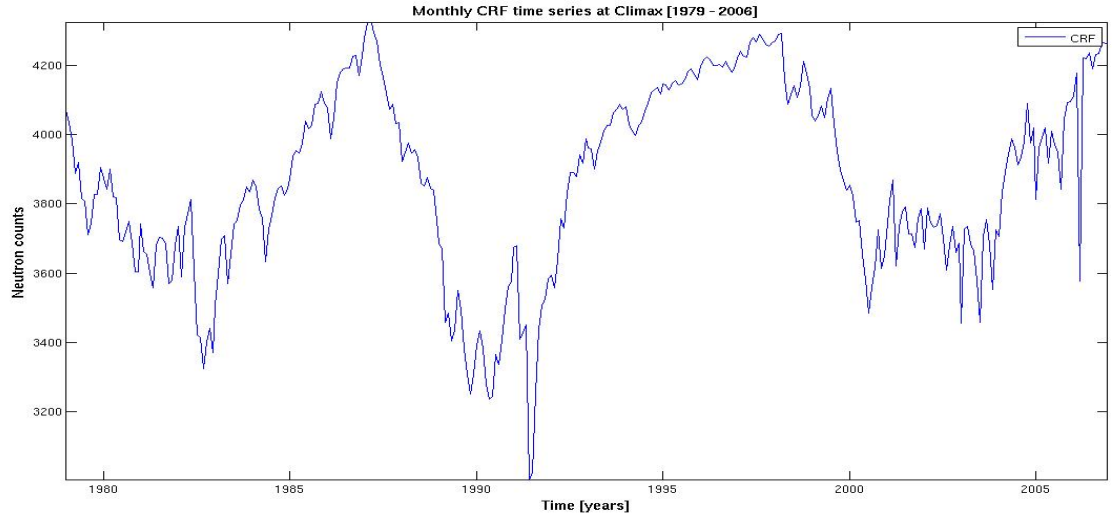

Figure 2: Time series plot of absolute CRF at Climax[1979 - 2006]

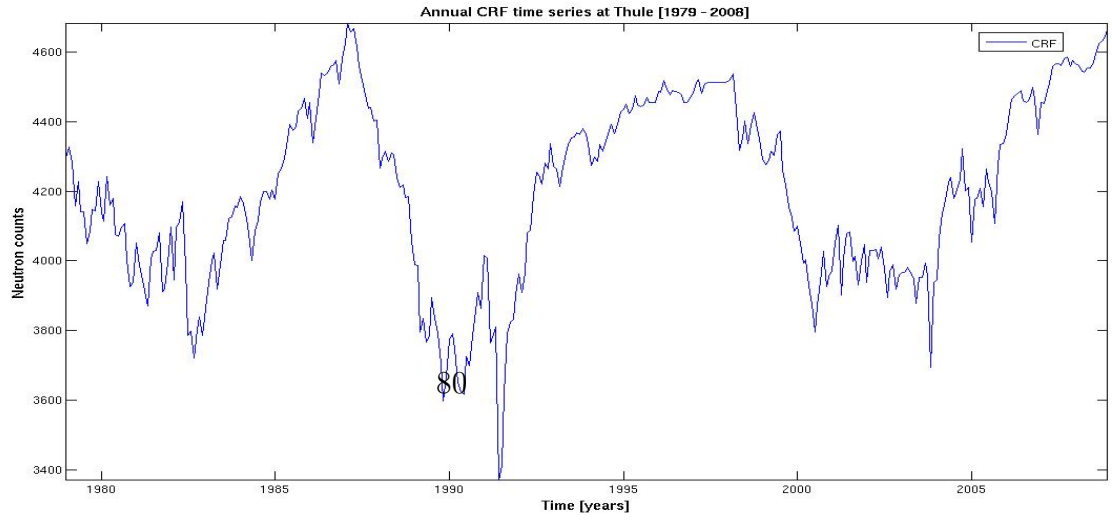

Figure 3: Time series plot of absolute CRF at Thule[1979 - 2008]

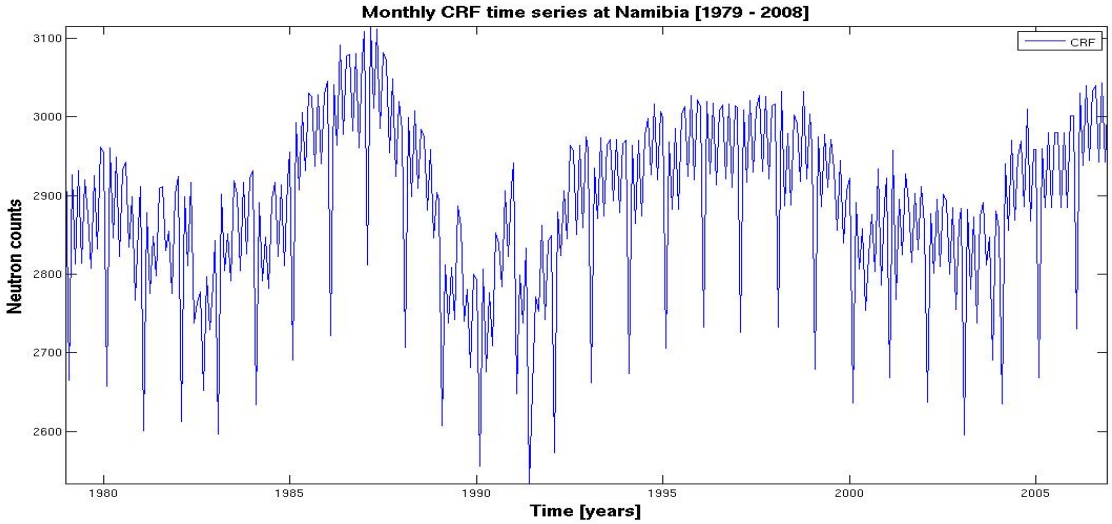

Figure 4: Time series plot of absolute (without scaling or normalization) CRF at Namibia[1979 - 2008]

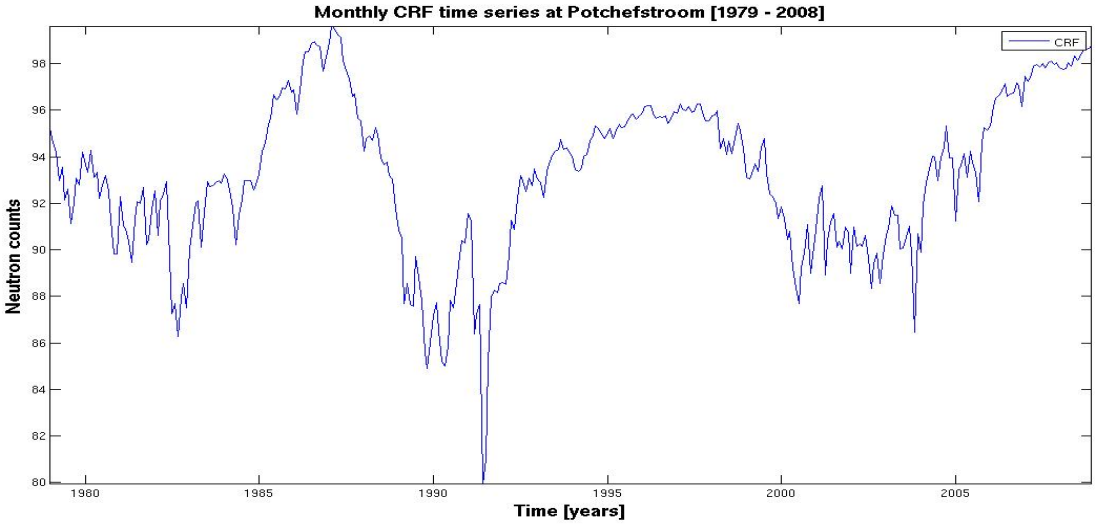

Figure 5: Time series plot of absolute (without scaling or normalization) CRF at Potchefstroom[1979 - 2008]

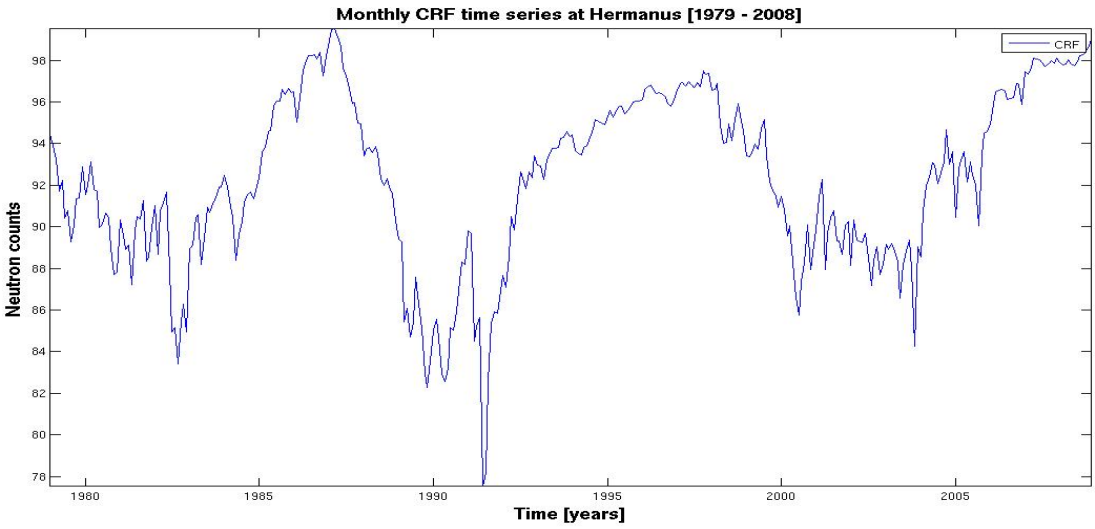

Figure 6: Time series plot of absolute (without scaling or normalization) CRF at Hermanus[1979 - 2008]